ESRRB Inhibits the TGFβ Signaling Pathway to Drive Cell Proliferation in Cervical Cancer

Qin-Shu Li[1] and Peng-Sheng Zheng[1,2]

ABSTRACT

Estrogen-related receptor β (ESRRB) is a member of the orphan nuclear receptor family and mediates stem cell self-renewal and early embryonic development. Previous studies have also reported that ESRRB plays a role in the development and progression of breast cancer and prostate cancer. In this study, we observed that ESRRB was highly expressed in cervical cancer and was associated with disease progression. Knocking out ESRRB using CRISPR/Cas9 gene editing in cervical cancer cells induced cell-cycle arrest at the transition from the G_0–G_1 phase to the S phase, resulting in inhibition of cell proliferation *in vitro* and reduced tumor growth *in vivo*. Conversely, ectopic expression of ESRRB significantly promoted the proliferation of cervical cancer cells. ESRRB activated transcription of SMAD7, a TGFβ pathway inhibitor, which blocked phosphorylation and nuclear translocation of SMAD2/3 to the nucleus, thereby downregulating CDKN1A and upregulating CCNA2 and MYC. In turn, MYC transactivated *ESRRB* and upregulated SMAD7, thus forming a positive feedback loop with ESRRB. Together, these findings identify the tumor-promoting function of ESRRB in cervical cancer and reveal a mechanism by which ESRRB stimulates cell proliferation to promote cancer progression.

Significance: The ESRRB/SMAD7/MYC-positive feedback loop inhibits TGFβ signaling to activate cell-cycle progression and promote proliferation in cervical cancer, thereby driving tumor growth.

Introduction

Existing data have shown that cervical cancer ranks as the fourth most common female tumor worldwide and the second leading cause of cancer-related deaths among women in developing countries (1). Persistent infection with high-risk subtypes of human papillomavirus (HPV) is one of the leading causes of cervical cancer (2), of which, HPV-16 and HPV-18 are associated with 70% of invasive cervical cancers (3). HPV infects the basal cells of the squamous epithelium of the cervix, and the viral *E6* and *E7* gene products can cause genetic changes in the host genome, including the silence of tumor suppressor genes as well as the activation of oncogenes (4, 5). For example, E6/E7 proteins mediate the degradation of the tumor suppressor genes *TP53* and *Rb*, thereby activating the transcription factor E2F1 and interfering with cell-cycle regulation (6, 7). Using next-generation sequencing (NGS) technologies, several studies have characterized genome-wide alterations in both viral and host genomes upon HPV integration in cervical cancer. Several genomic hotspots that are potentially involved in cancer-related pathways were identified (8). For example, amplification of *YAP1* and *EGFR* was found in squamous carcinoma. Deletion of *TGFBR2* and *SMAD4* and amplification of *ERBB2* and *KLF5* were found in adenocarcinoma. MYC, HIF1A, and MAPK signaling pathways were identified as key distinguishing signaling features in squamous cell carcinoma of the cervix (9).

Estrogen-related receptor β (ESRRB) is a nuclear transcription factor. It consists of four domains, the A–B domain, the C domain (DNA binding domain), which mainly depends on two zinc finger structures to bind to estrogen response element or estrogen-related response element (ERRE) to activate the expression of target genes (10), the D domain (hinge region), and the E domain (ligand binding domain; ref. 11). ESRRB mediates self-renewal and pluripotency in embryonic stem cells (ESC). It plays an important role in recruiting the core pluripotency factors OCT4, SOX2, and NANOG during the reprogramming of epiblast stem cells (12). OCT4, SOX2, and NANOG are highly expressed in cancer stem cells (CSC; ref. 13). CSCs play major roles in tumor initiation, progression, and resistance to cancer therapy (14). Therefore, ESRRB, as a pluripotent central regulatory molecule, may play an important role in the development and progression of tumors. The role of ESRRB in breast and prostate cancers has been previously described. Specifically, ESRRB is downregulated in breast cancer cells, and its overexpression in patients with breast cancer is positively correlated with an improved prognosis and prolonged relapse-free survival (15). ESRRB can inhibit the growth of prostate cancer cells *in vivo* and *in vitro*, and is therefore considered a potential therapeutic target for prostate cancer patients (16). One study suggests that ESRRB agonists may overcome glucocorticoid resistance in acute lymphoblastic leukemia (ALL) and induces leukemia cell death in synergy with glucocorticoid (17). The expression of ESRRB has been detected in ovarian cancer, but there are no significant differences compared with normal ovarian tissues (18). To date, the expression and the role of ESRRB in cervical cancer have not been reported.

Here, we found that ESRRB was highly expressed in cervical cancer tissues compared with normal cervix tissues. Our data suggest that ESRRB promotes the proliferation of cervical cancer cells *in vitro* and *in vivo* by inhibiting the TGFβ pathway through transactivating *SMAD7*. In turn, MYC, downstream of the TGFβ pathway, can

[1]Department of Reproductive Medicine, The First Affiliated Hospital of Xi'an Jiaotong University, Xi'an, Shaanxi, P.R. China. [2]Section of Cancer Stem Cell Research, Key Laboratory of Environment and Genes Related to Diseases, Ministry of Education of the People's Republic of China, Xi'an, Shaanxi, P.R. China.

Corresponding Author: Peng-Sheng Zheng, Director and Professor, Department of Reproductive Medicine, The First Affiliated Hospital of the Medical College, Xi'an Jiaotong University, 76 West Yanta Road, Xi'an, Shaanxi Province, 710061, P.R. China, Phone: 86-029-82657874; Fax: 86-029-85324013; E-mail: zpsheng@mail.xjtu.edu.cn

Cancer Res 2023;83:3095–114

doi: 10.1158/0008-5472.CAN-23-0067

transactivate *ESRRB* and upregulate SMAD7, forming a positive feedback loop with ESRRB to strengthen the function of ESRRB. Therefore, ESRRB may be considered one of the key factors in the development of cervical cancer.

Materials and Methods

Human tissue specimens

Thirty-one normal cervix (NC) tissues, 21 cervical high-grade intraepithelial neoplasia (HSIL) tissues, and 64 cervical carcinoma tissues were collected from the First Affiliated Hospital of Xi'an Jiaotong University. NC tissues were obtained from patients undergoing total myomectomy. Cervical carcinoma tissues were obtained from cervical cancer patients who had not received chemotherapy, immunotherapy, or radiotherapy. All tissues were immediately frozen in liquid nitrogen for subsequent experiments. Histologic classification and clinical staging were performed in accordance with the International Federation of Gynecology and Obstetrics (FIGO) classification system. The study was conducted in accordance with the Declaration of Helsinki, which is a recognized ethical guideline. The Institutional Review Board of the Ethics Committee of the School of Medicine of Xi'an Jiaotong University, China, approved the study (No. 2014-113). All procedures followed approved medical ethical practices and all patients were written informed consent before specimen collection.

IHC and immunocytochemistry

The IHC and immunocytochemistry staining procedures were performed as previously described (19). Immune reactivity score (IRS) is calculated using the following formula: IRS = intensity score × quantity score. Quantity score represents the percentage of ESRRB-positive staining cells. We randomly observed the five different visual fields of the tissue section and took the average of the five different visual fields as the final score of the section. The score can be divided into five grades: 0, <10%; 1, 10%–25%; 2, 25%–50%; 3, 50%–75%; and 4, >75%. The intensity score represents the staining intensity. We randomly observed five different visual fields of the tissue section and took the average intensity of the five different visual fields as the final score of the tissue section. The score can be divided into four grades: nonstaining, 0; light brown, 1; brown, 2; and dark brown, 3. ESRRB staining was classified into three categories: negative, weakly positive, and strongly positive. IRS ≤3 is defined as negative, >3 but ≤6 as weakly positive, and >6 as strongly positive. At least two different pathologists evaluated all specimens by blind method. The antibodies used were as follows: anti-ESRRB (1:200 dilution, # PP-H6705-00, R&D Systems, RRID:AB_2100412), anti-Ki67 (1:200 dilution, #sc-23900, Santa Cruz, RRID:AB_627859), anti-CDKN1A (1:300 dilution, #2947, Cell Signaling Technology, RRID:AB_823586), anti-CCNA2 (1:300 dilution, #WL02964, Wanleibio), and anti-MYC (1:300 dilution, #10828-1-AP, Proteintech, RRID:AB_2148585), anti-pSMAD2$^{Ser465/467}$ (1:50 dilution, #18338, Cell Signaling Technology, RRID:AB_2798798), anti-pSMAD3$^{Ser423/425}$ (1:50 dilution, #ab52903, Abcam, RRID: AB_882596), anti-SMAD4 (1:200 dilution, #sc-7966, Santa Cruz, RRID:AB_627905), anti-SMAD7 (1:300 dilution, #ab272928, Abcam, RRID:AB_2924382).

Western blotting

For nuclear protein extraction, the Nuclear and Cytoplasmic Protein Extraction Kit (#78833, Thermo Scientific) was used. Clinical tissues or cells were lysed in lysis buffer containing freshly added protease inhibitors (#04693116001, Roche Diagnostics) for 30 minutes on ice, then supernatants were extracted by centrifugation for 15 minutes at 4°C and quantified by protein concentration determination using a bicinchoninic acid assay (BCA, Thermo Scientific), after which the proteins were denatured by adding 5× loading buffer and boiling at 95°C for 5 minutes. Equal amounts of protein were separated by using SDS-PAGE and blotted onto activated 0.45-μm pore size PVDF membrane (Millipore). After blocking in 5% nonfat milk for 1 hour, the membranes were incubated with primary antibodies overnight at 4°C under gentle agitation, the secondary antibodies used HRP-conjugated anti-rabbit (1:10,000 dilution) or anti-mouse (1:5,000 dilution) IgG (Thermo Fisher Scientific). Finally, Proteins were visualized by ECL enhanced chemiluminescence solution (Millipore). The signal intensity was detected using the protein imprinting imaging system (Tanon 5200). Quantitative analysis of strips was conducted on ImageJ software: The gray value of the target protein was divided by the gray value of the GAPDH to indicate the expression level of the target protein. The antibodies used were as follows: anti-ESRRB (1:1,000 dilution, #PP-H6705-00, R&D Systems), anti-CDKN1A (1:300 dilution, #2947, Cell Signaling Technology), anti-CCNA2 (1:500 dilution, #WL02964, Wanleibio), and anti-MYC (1:1,000 dilution, #10828-1-AP, Proteintech), anti-SMAD2 (1:1,000 dilution, #5339, Cell Signaling Technology, RRID:AB_10626777), anti-pSMAD2$^{Ser465/467}$ (1:50 dilution, #18338, Cell Signaling Technology), anti-SMAD3 (1:300 dilution, #9523, Cell Signaling Technology, RRID: AB_2193182), anti-pSMAD3$^{Ser423/425}$ (1:200 dilution, #ab52903, Abcam), anti-SMAD4 (1:500 dilution, #sc-7966, Santa Cruz), anti-SMAD7 (1:300 dilution, #ab272928, Abcam), anti-GAPDH (1:1,000 dilution, #sc-47724, Santa Cruz, RRID:AB_627678), anti-lamin B1 (1:300 dilution, sc-56144, Santa Cruz, RRID:AB_784272).

Cervical cancer cell lines, cell culture, and drug treatments

HeLa (cat. # CC-L2, RRID: CVCL_0030), SiHa (cat. # HTB-35, RRID: CVCL_0032), C-33A (RRID: CVCL_1094), CaSki (RRID: CVCL_1100), and HT-3 (RRID: CVCL_1293) were purchased from the ATCC in 2019. Ect/E6E7 was purchased from GuanDao (#20200806-01, GuanDao) in 2020. HeLa, SiHa, and C33A cells were cultured in DMEM (Sigma-Aldrich); CaSki cells were cultured in RPMI-1640 (Sigma-Aldrich); HT-3 cells were cultured in McCoy's 5A medium (Sigma-Aldrich); Ect1/E6E7 cells were cultured in MEM medium (Sigma-Aldrich). All media were supplemented with 10% heat-inactivated fetal bovine serum (HyClone) and 1% penicillin–streptomycin. All cell lines were maintained at 37°C with 5% CO_2. Cell lines were authenticated within 2 years using short tandem repeat analysis as described in 2012 in ANSI Standard (ASN-0002) by the ATCC Standards Development Organization and in Capes-Davis and colleagues match criteria for human cell line authentication. All new cells were tested free of *Mycoplasma* contamination using RT-PCR. The cumulative culture length of the cells between thawing and used in this study was fewer than 10 passages. To explore the effect of MYC on ESRRB expression, HeLa and SiHa cells were treated with different concentrations of 10058-F4 (#S7153, Selleck), inhibitor of MYC, for 24 hours (20). ESRRB-knockout cells treated with SB525334 (#S1476, Selleck), inhibitor of pSMAD2$^{Ser465/467}$ and pSMAD3$^{Ser423/425}$, for 24 hours at a concentration of 2 μm (21).

PCR, quantitative RT-PCR

As previously described (19), total RNA was isolated using TRIzol reagent (Invitrogen). Briefly, samples were treated with 20% chloroform, vortexed, and centrifuged for 15 minutes. The upper aqueous phase (containing RNA) was collected and an equal volume of isopropanol was added, followed by a centrifugation step for 15 minutes.

The RNA pellet was washed with 75% ethanol, air-dried, and then recovered in RNase-free water. The RNA template was converted to cDNA using PrimeScript RT Reagent Kit (Perfect Real Time; TaKaRa). The cDNA was then used as a template for PCR amplification using PrimeSTAR HS DNA Polymerase (Takara) or for quantitative RT-PCR (qRT-PCR) using SYBR Green Master Mix (TaKaRa). The C_t value was detected using the qRT-PCR instrument (Gentier 96E/96R, TIANLONG). GAPDH was used as an internal control to calculate the expression of the target genes: $\Delta C_t = C_t$ (target genes) $- C_t$ (GAPDH). The relative expression of the experimental groups was calculated by the comparative $2^{-\Delta\Delta C_t}$ method. Primer sequences are listed in Supplementary Table S2.

RNA sequencing

Total RNA was isolated from the three biological replicates of HeLa-sgCtrl and the HeLa-sgEsrrb cells with TRIzol reagent according to the manufacturer's instructions (Invitrogen). RNA quality was assessed using a 2100 Expert Bioanalyzer (Agilent) and sent for mRNA library construction and sequencing using the DNBSEQ-500 platform of the Beijing Genomics institution. The data were analyzed on the free online Dr. Tom Platform (https://biosys.bgi.com/#/report/login). The results of the RNA-seq analysis have been uploaded to the Gene-Expression Omnibus (GEO) database, and the access number is GSE229349.

Vector construction and transfection

All primers used are listed in Supplementary Table S2. We used the website http://crispr-era.stanford.edu/ to select the single guide RNA (sgRNA) with the highest score targeting the fourth exon of ESRRB, and inserted the double strand DNA of sgEsrrb formed after annealing into the pSpCas9 (BB) - 2A-GFP plasmid (plasmid # 68370, Addgene). The vector contains a green fluorescent gene. Next, we used flow sorting to select HeLa and SiHa cells expressing green fluorescent protein and then cells were planted into 96-well plates to form monoclonal and then amplify it. Then, the genomic DNA of the cloned cells was extracted using TIANamp Genomic DNA Kit (Tiangen). The primer of the fourth exon of ESRRB is used to amplify the flanking segment of the sgRNA binding site in the genomic DNA. After purification of the PCR product, the T7E1 experiment (#M0302S, NEB) verifies the cutting efficiency. Then, the purification of the PCR product was verified by Sanger sequencing (Tsingke) and the genotypes of different clones were analyzed. We selected clones with ESRRB homozygous knocked out at the genomic level to further verify their knockout efficiency at the protein level with Western blotting. The cells that successfully knock out of ESRRB (HeLa-sgEsrrb and SiHa-sgEsrrb) and the corresponding control cells (HeLa-sgCtrl and SiHa-sgCtrl) were used for subsequent experiments.

Human full-length ESRRB (NM_004452.4) cDNA was amplified from HeLa cDNA library and subsequently cloned into the EcoR1 and Xhol (TaKaRa) sites of an internal ribosome entry site vector, pIRES2-mCherry-Neo (Clontech) to generate the recombinant pIRES2-mCherry-Neo-ESRRB plasmid and transfect it into HeLa-sgEsrrb cells. Successful transfection was verified as mCherry fluorescence under a fluorescence microscope. Then, G418 (Calbiochem) with a concentration of 1 mg/mL was added for 2–3 weeks to screen the cells that were successfully transferred into the ESRRB overexpression plasmid, and identified by Western blotting. These cells were named HeLa-sgEsrrb-Esrrb^{OE}. The construction method of SMAD7 and MYC overexpression plasmid is roughly the same as above.

For the dual-luciferase reporter gene plasmid, primers were designed for a sequence of 2,000 bp upstream and 500 bp downstream of the transcription start site and other truncated fragment primers were designed according to different fragment lengths. PCR amplification was performed from genomic DNA, and then cloned to the MluL and BgI II (TaKaRa) sites of the internal ribosome entry site vector pGL3 Basic luciferase vector (Addgene, RRID: Addgene 48743) to generate a recombinant PGL3-SMAD7 luciferase vector. The construction method of ESRRB dual-luciferase reporter plasmid is roughly the same as above. pGL3-SBE4-Luc was a gift from Dr. Qingmei Liu (National Ministry of Education Key Laboratory of Contemporary Anthropology, School of Life Sciences, Fudan University, Shanghai, PR China), which consisted of four short tandem repeats of SMAD binding element (SBE; GTCTAGAC) with a minimal promoter (TATA box). The plasmid of pRL-SV40 was used as an internal control (22). See Supplementary Table S2 for details of primers.

Each cell line was transfected with the indicated plasmid using Lipofectamine 2000 reagent (Invitrogen) according to the manufacturer's instructions.

Cell proliferation and cell cycle and apoptosis assays

In vitro cell proliferation was evaluated by CCK-8 and cell counting. Cell viability was assessed at specific time points using the CCK-8 Kit (#C0005, TargetMol). Cells were plated at a density of 1,000 cells in 96-well plates, and CCK-8 was added to each well for 7 days according to the manufacturer's instructions. OD was determined at 450 nm using BioTek Microplate Instrumentation. In the cell counting test, 2×10^4 cells were seeded in 6-well plates and cultured for 7 days, and counted every 2 days. Cells were harvested and fixed with 70% cold ethanol for cell-cycle assay. After rinsing 2-3 times with PBS, the cells were stained with solutions containing PI and DNase-free RNase A (Sigma-Aldrich) for 30 minutes in the dark. For the apoptosis assay, cells were washed twice with cold PBS and then resuspend cells in 1× binding buffer, incubated with PE Annexin V and 7-AAD (TDS559763, BD Biosciences) for 15 minutes in the dark at room temperature, and were analyzed by flow cytometry. Cell-cycle and apoptosis analysis were run on a FACSCanto II flow cytometer (BD Biosciences) using CellQuest software (RRID:SCR_014489). The results were analyzed with FlowJo_V10 cell analyzer.

Subcutaneous tumorigenesis test in nude mice

The mice used in this study (4–5-week-old BALB/c nude female, RRID: IMSR_ORNL: BALB/cRl) were from Shanghai SLAC Experimental Animal Co, Ltd. All procedures are carried out in accordance with the "Principles of Experimental Animal Care" (NIH) and "The Animal Research: Reporting of *In Vivo* Experiments" (ARRIVE) and the guidelines of Xi'an Jiaotong University Laboratory Animal Care Committee (2016-117). The Experimental Animal Ethics Committee of Xi'an Jiaotong University approved the study. Animals had free access to food and water and were housed with a 12-hour light–dark cycle and constant temperature under specific pathogen-free conditions. We collected 8×10^5 HeLa-sgEsrrb and SiHa-sgEsrrb cells, respectively. The same number of control cells was also collected. HeLa-sgCtrl and HeLa-sgEsrrb cells were injected subcutaneously into each side of the back of each mouse (200 μL of cells per site), respectively. Similarly, SiHa-sgCtrl and SiHa-sgEsrrb, HeLa-sgEsrrb-Esrrb^{OE} and its control cells were inoculated in the same amount. Each group had 6 replicates. The length and width of the xenograft tumor were measured manually with a caliper every 2–3 days. The tumor volumes were calculated as follows: $V = 0.52 \times \text{length} \times \text{width}^2$. In the same group of mice, when any diameter of the subcutaneous tumor is closed to 1.5 cm, all the mice will be killed. The tumors were stripped

and weighed and finally photographed by iPhone. For the tumor-free interval curve, we evaluated the xenograft tumor every 2-4 days, recorded the time interval of occurrence of palpable tumors, and conducted Kaplan–Meier survival analysis.

Dual-luciferase reporter assay

The promoter region of the SMAD7 and ESRRB was inserted into the predigested pGL3-basic luciferase vector (Promega) to produce luciferase reporter plasmids pGL3-SMAD7-Luc and pGL3-ESRRB-Luc. The constructs were verified by Sanger sequencing (Tsingke). Primers for plasmid constructs are shown in Supplementary Table S2. 10×10^4 HeLa-sgEsrrb, SiHa-sgEsrrb, and HeLa-sgEsrrb-Esrrb^{OE}, and their control cells were inoculated into 24-well culture plates. Lipofectamine 2000 (Invitrogen) was used for cotransfection with pGL3-SMAD7-Luc and pRL-TK plasmids (Promega) in the above cells. 293T cells were cotransfected with pGL3-SMAD7-Luc and pRL TK plasmids. Then, these 293T cells have been transfected with pSpCas9 (BB)-2A-GFP-sgEsrrb and its control vector, respectively. In addition, HeLa cells were cotransfected with pGL3-ESRRB-Luc and pRL-TK plasmids (Promega). These HeLa cells have been transfected with pIRES2-AcGFP-Neo-MYC and its control vector, respectively. Cells were harvested 48 hours after transfection, and luciferase activities were analyzed on the full wavelength multifunctional microplate reader (Varioskan Flash, Thermo Scientific) using a dual-luciferase reporter assay system (Promega). Data are shown as relative luciferase activity (Firefly luciferase activity/*Renilla* luciferase activity) and then converted to fold change in the experimental group relative to the control group. Each experiment was conducted in triplicate. Primers are shown in Supplementary Table S2. pGL3-SBE4-Luc and pRL-SV40 (internal control) were also transfected and analyzed in a broadly similar way.

Chromatin immunoprecipitation qPCR assay

Chromatin immunoprecipitation (ChIP) assay can be performed using the SimpleChIP Enzymatic Chromatin IP Kit (#9003s, Cell Signaling Technology) according to the manufacturer's standard protocol. Briefly, indicated cells were fixed with 1.0% formaldehyde for 15 minutes at room temperature and then glycine was added to the medium. The cells were then lysed and stored at −80°C until use. Chromatin was fragmented to an average length of 300 bp by ultrasound (VCX150). The diluted chromatin fragments were incubated overnight at 4°C with 5 μg anti-ESRRB (#PP-H6705-00, R&D Systems), anti-MYC (#10828-1-AP, Proteintech), and anti-IgG (negative control) antibody. The immunoprecipitated supernatant was pulled down using fully resuspended protein A/G magnetic beads. Finally, the immunoprecipitate was collected, washed, and the DNA was purified. Purified DNA fragments were used as templates for qPCR analysis, and data were normalized with 2% input. Primers are shown in Supplementary Table S2.

Statistical analysis

Statistical analyses were performed using GraphPad Prism 8.0 software (RRID:SCR_002798) and SPSS 18.0 software (SPSS, Inc., RRID:SCR_002865). Values were expressed as mean ± SD for continuous variables and as frequencies and proportions for categorical variables. Student *t* test (between two groups) and one-way ANOVA (more than two groups) were used to analyze continuous variables with normal distribution and the χ^2 test or one-way ANOVA was performed for comparisons among groups. Survival-free interval curves were calculated according to the Kaplan–Meier method, and analysis was performed using the log-rank test. The correlation of the two genes was analyzed by the Spearman rank test. Each experiment was repeated in triplicate or more times under identical or similar conditions, and $P < 0.05$ was considered statistically significant. Cell samples were randomly selected for transfection into the appropriate vectors and reagents, and the cell samples were randomly injected subcutaneously into the mice.

Data availability

The RNA-seq data generated in this study are publicly available in GEO at GSE229349. Survival analyses were performed with the Kaplan–Meier estimator from the Kaplan–Meier plotter (http://kmplot.com/analysis/). Transcription factor binding site map was obtained from the JASPAR database (https://jaspar.genereg.net/). All other raw data are available upon request from the corresponding author.

Results

Upregulation of ESRRB is associated with the progression of human cervical cancer

Pan-cancer analysis was performed to compare the expression of ESRRB in tumor tissues and normal tissues (Supplementary Fig. S1A). To explore the role of ESRRB in the development and progression of cervical cancer, we determined ESRRB expression in NC ($N = 31$) tissues, HSILs ($N = 21$), and cervical carcinoma ($N = 64$) tissues using IHC. ESRRB staining was classified into three categories: negative, weakly positive, and strongly positive. As shown in **Fig. 1A**. ESRRB-positive staining areas were mainly distributed in the nucleus of NC, HSIL, and CC, with a small distribution in the cytoplasm. The percentage of strongly positive ESRRB staining was 6.5% in NC (2/31), 19.0% in HSIL (4/21), and 39.1% in cervical carcinoma (25/64). The percentage of weakly positive ESRRB staining was 16.1% in NC (5/31), 28.6% in HSIL (6/21), and 18.8% in cervical carcinoma (12/64). The percentage of negative ESRRB staining was 77.42% in NC (24/31), 52.38% in HSIL (11/21), and 42.19% in cervical carcinoma (27/64; **Fig. 1B**; Supplementary Table S1; $P < 0.05$). Moreover, the immunoreactivity score (IRS) of ESRRB staining increased from 2.03 ± 2.48 in NC to 3.81 ± 3.52 in HSIL and then to 4.97 ± 3.81 in cervical carcinoma (**Fig. 1C**, $P < 0.0001$). Next, we randomly selected eight NC samples and eight cervical carcinoma samples and analyzed the expression of ESRRB in these tissues using Western blotting. We found that the expression of ESRRB in cervical carcinoma samples was higher than that in NC samples (**Fig. 1D** and **E**, $P < 0.05$). Collectively, these observations suggest that ESRRB may play a role in the development and progression of cervical cancer.

ESRRB enhances cervical cancer cell growth *in vivo*

To further elucidate the role of ESRRB in the development and progression of cervical cancer, we examined the expression of ESRRB in cervical cancer cell lines at the protein level. As shown in **Fig. 2A** and **B**, ESRRB was generally highly expressed in cervical cancer cell lines (HeLa, SiHa, C33-A, CaSki, and HT-3) but not in a human normal ectocervical cell line (Ect1/E6E7). ESRRB-positive staining areas were mainly distributed in the nucleus of cervical cancer cell lines, with a small distribution in the cytoplasm. Based on the expression of ESRRB in cervical cancer cell lines, we constructed and screened monoclonal cells with the stable knockout of ESRRB in HeLa and SiHa cells using CRISPR/Cas9 technology (HeLa-sgEsrrb and SiHa-sgEsrrb). As ESRRB was commonly highly expressed in cervical cancer cell lines, we constructed and screened monoclonal cells with stable overexpression of ESRRB in HeLa-sgEsrrb cells

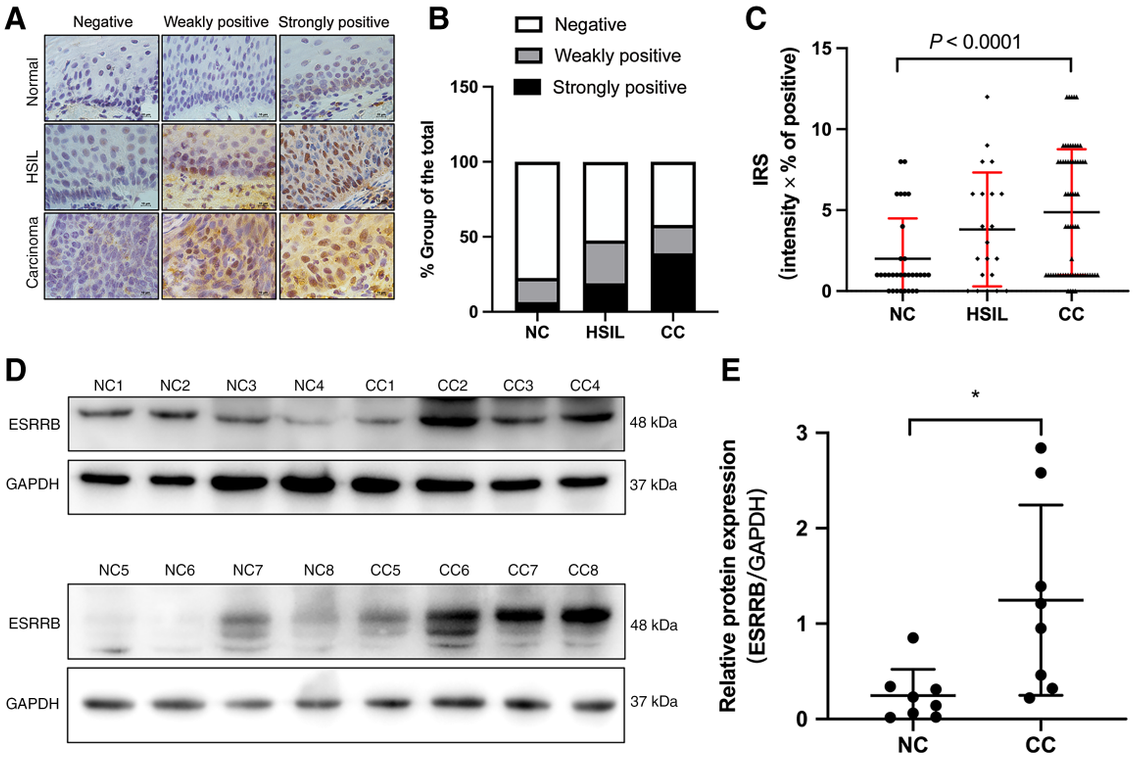

Figure 1.

Upregulation of ESRRB is associated with the progression of human cervical cancer. **A,** IHC analysis of ESRRB expression using ESRRB antibody in 31 normal cervix (NC) samples, 21 high-grade squamous intraepithelial lesions (HSIL), and 64 cervical carcinoma (CC) samples. Representative images are shown. Scale bar, 10 μm. **B,** Histogram shows the proportion of negative, weakly positive, and strongly positive ESRRB staining in NC, HSIL, and CC groups, respectively. **C,** IRS was used to compare ESRRB IHC staining between NC, HSIL, and CC groups. One-way ANOVA was used to analyze the data. **D** and **E,** The protein levels of ESRRB in 8 normal cervix samples and 8 cervical carcinoma samples from cervical cancer patients (biological replicates = 8). The Western blotting bands were quantified and normalized to GAPDH to indicate relative levels of ESRRB expression. Data, mean ± SD. *, $P < 0.05$ vs. the control group.

(HeLa-sgEsrrb-Esrrb^{OE}). The knockout and overexpression efficiency were confirmed by qRT-PCR and Western blotting (**Fig. 2C**; Supplementary Fig. S1B, $P < 0.01$). To explore the effect of ESRRB on cervical cancer tumorigenesis *in vivo*, we performed a subcutaneous tumorigenesis assay in female nude mice. A total of 8×10^5 HeLa-sgEsrrb was injected subcutaneously into one side of the back of immune-deficient BALB/c mice to assess the tumor formation potential. The same number of control cells corresponding to HeLa-sgEsrrb was injected subcutaneously into the other side of the back of BALB/c mice (**Fig. 2D**). Compared with the control group, knocking out ESRRB in HeLa cells caused a significant inhibition in tumor volume and tumor weight (**Fig. 2E**, $P < 0.05$). A similar result was obtained in SiHa-sgEsrrb (**Fig. 2F** and **G**, $P < 0.05$). Additionally, the mice in the ESRRB-knockout groups showed a longer tumor-free survival than those in the control groups (Supplementary Fig. S1C, $P < 0.05$). Conversely, ESRRB overexpression in HeLa-sgEsrrb remarkably elevated tumor volume and tumor weight in nude mice (**Fig. 2H** and **I**, $P < 0.05$) and shortened tumor-free survival (Supplementary Fig. S1D, $P < 0.05$). Taken together, these data support the oncogenic role of ESRRB in cervical cancer *in vivo*.

ESRRB promotes the proliferation and cell-cycle progression of cervical cancer cells *in vitro*

Next, the tumor xenograft tissues were stained with Ki67, which is a reliable marker of tumor cells' proliferative activity. The results showed that IRS of Ki67 staining was significantly decreased in tumor xenograft tissues formed by HeLa-sgEsrrb or SiHa-sgEsrrb compared with that in tumor xenograft tissues formed by their control cells. In contrast, IRS of Ki67 staining was significantly increased in tumor xenograft tissues formed by HeLa-sgEsrrb-Esrrb^{OE} compared with that in tumor xenograft tissues formed by its control cells (**Fig. 3A** and **B**, $P < 0.05$). This suggests that ESRRB may be tumorigenic by affecting the proliferative activity of cervical cancer cells. Therefore, we used cell counting, Cell Counting Kit-8 (CCK8), and cell-cycle assays to explore the effect of ESRRB on the proliferation of cervical cancer cells *in vitro*. The data showed that HeLa-sgEsrrb exhibited markedly decreased cell proliferation and viability compared with HeLa-sgCtrl (**Fig. 3C**, $P < 0.05$). A similar result was obtained in SiHa-sgEsrrb (**Fig. 3D**, $P < 0.05$). Conversely, ESRRB overexpression in HeLa-sgEsrrb markedly rescued cell proliferation and viability relative to control cells (**Fig. 3E**, $P < 0.05$). Additionally, we performed cell-cycle assays using flow cytometry, and the results showed a statistically significant increase in the percentage of cells in the G_1–G_0 phase and a decrease in the percentage of cells in the S phase in HeLa-sgEsrrb relative to that in control cells (**Fig. 3F**, $P < 0.01$). A similar result was obtained in SiHa-sgEsrrb (**Fig. 3G**, $P < 0.05$). However, HeLa-sgEsrrb with stable overexpression of ESRRB accelerated the cell-cycle transition, leading to a decrease in the percentage of cells in G_0–G_1 phase and an increase in the percentage of cells in the S phase compared with

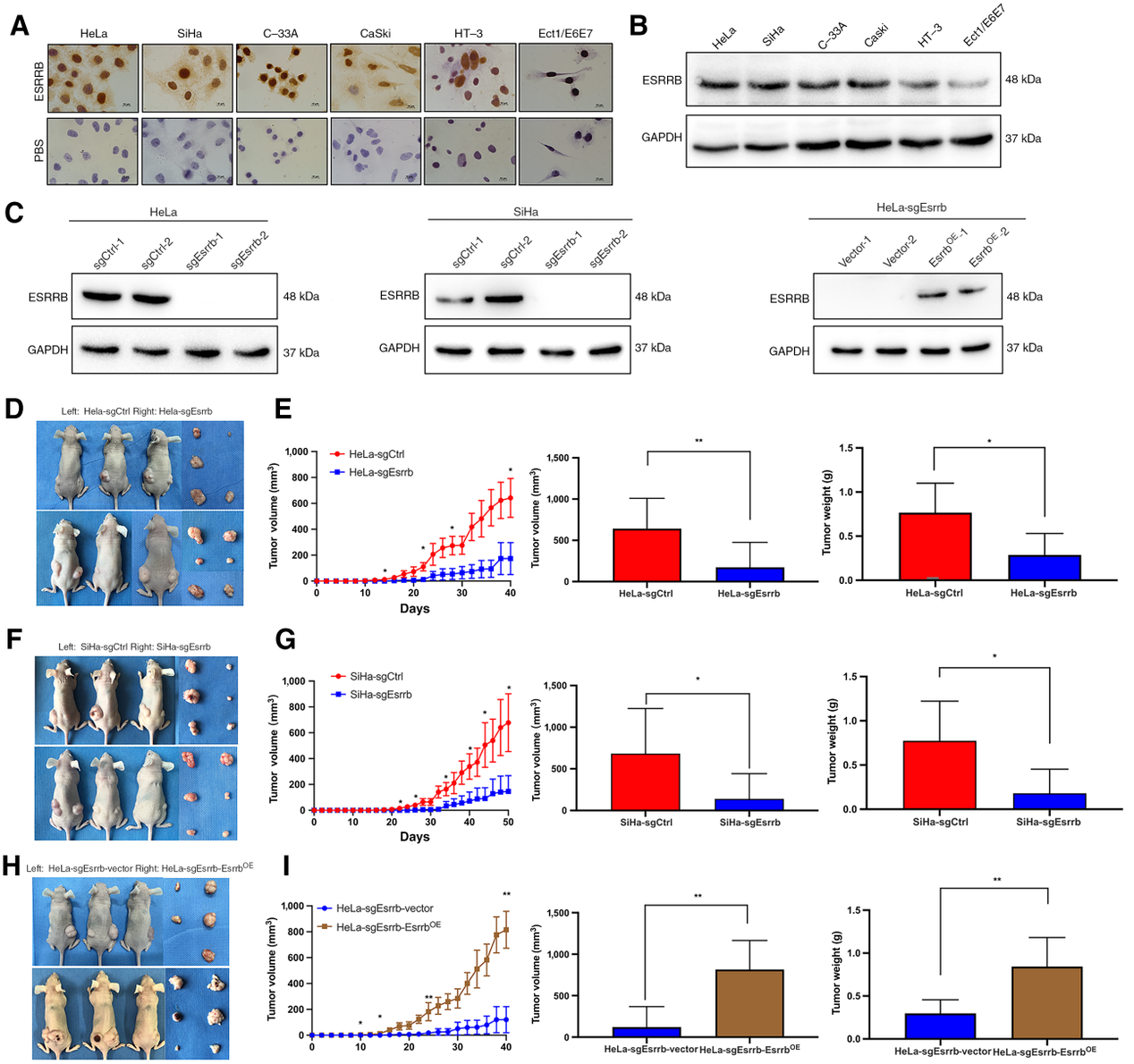

Figure 2.

ESRRB enhances cervical cancer cell growth *in vivo*. **A** and **B,** Western blotting and ICC showed the expression of ESRRB in five cervical cancer cell lines and human cervical immortalized squamous cells. PBS was used in place of primary antibody to exclude some nonspecific staining. Representative images are shown. Scale bar, 10 μm. **C,** The knockout efficiency of ESRRB was determined by Western blotting in HeLa and SiHa cells, and overexpression efficiency of ESRRB was also determined in HeLa-sgEsrrb cells (biological replicates = 3; right). **D,** Mice bear xenografts from HeLa cells with stable ESRRB knockout and their control, respectively. **E,** The growth curves of xenografts derived from HeLa-sgEsrrb cells and its control cells were analyzed and histograms show quantitative analysis of the volume and weight of the tumor after dissection (biological replicates = 6 per group). **F** and **G,** The growth of xenografts derived from SiHa-sgEsrrb cells and its control cells (biological replicates = 6 per group). **H,** HeLa-sgEsrrb cells in which overexpressing ESRRB and its control cells were subcutaneously injected into nude mice, respectively. **I,** The effect of ESRRB overexpression on tumor volume and tumor weight was observed (biological replicates = 6 per group). All data, mean ± SD. Student *t* test was used for statistical analysis. *, $P < 0.05$; **, $P < 0.01$.

control cells (**Fig. 3H**, $P < 0.05$). In addition, we tested the effect of ESRRB depletion on the apoptosis of cervical cancer cells. There were no significant differences in early apoptosis and late apoptosis between ESRRB-modified cells and their control cells (Supplementary Fig. S1E). Taken together, these findings indicate that ESRRB promotes cervical cancer cell proliferation and promotes cell cycle transition *in vitro*.

ESRRB facilitates cervical cancer cell proliferation by regulating cell cycle–related proteins

To clarify the mechanism by which ESRRB promotes the development and progression of cervical cancer, we used transcriptome sequencing (RNA-seq) to identify changes in the expression of other molecules following ESRRB knockout in HeLa cells. Sequencing results showed that 2,589 genes were differentially expressed between

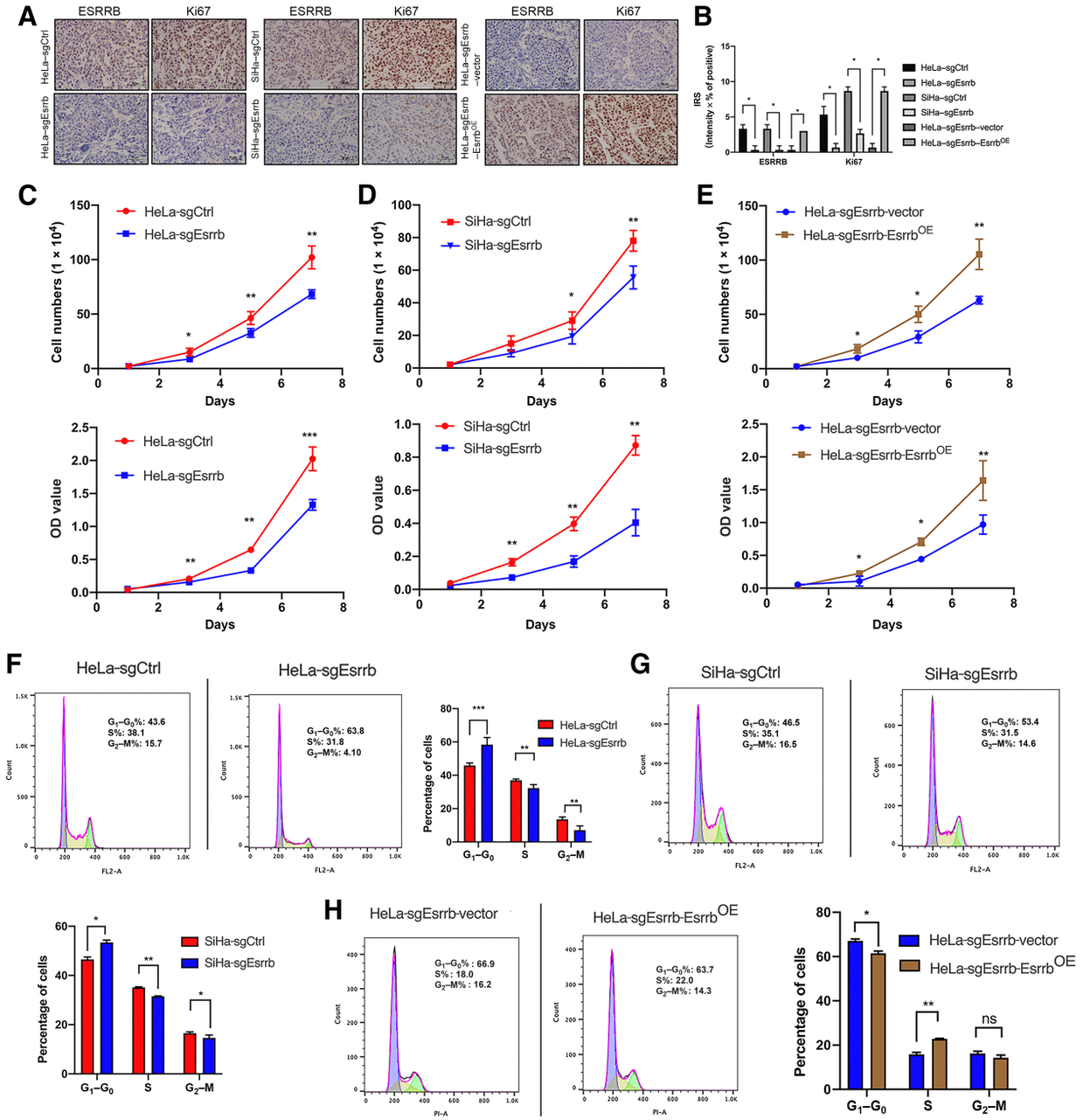

Figure 3.

ESRRB promotes the proliferation and cell-cycle progression of cervical cancer cells *in vitro*. **A** and **B,** Representative images of ESRRB and Ki67 staining of xenograft tumors from the indicated groups. Histogram shows the IRS of ESRRB and Ki67 in each group. Scale bar, 50 μm. **C** and **D,** The effect of ESRRB deficiency on HeLa and SiHa cell proliferation was assessed by the CCK8 assay and cell counting assay. **E,** CCK8 and cell counting assay showed the effect of ESRRB overexpression on the cell proliferation of HeLa-sgEsrrb cells. **F–H,** Cell-cycle profiles were analyzed by FACS in ESRRB-knockout HeLa (**F**) and SiHa (**G**) cells, as well as in HeLa-sgEsrrb-Esrrb^{OE} (**H**) cells. Representative images are shown. All data, mean ± SD. Student *t* test was used for statistical analysis. *, $P < 0.05$; **, $P < 0.01$; ***, $P < 0.001$. All data represent at least three independent experiments. (**F–H,** Created with FlowJo software.)

HeLa-sgCtrl and HeLa-sgEsrrb, including 1,540 genes that were upregulated and 1,049 genes that were downregulated (Supplementary Fig. S2A). Functional analysis of the differentially expressed genes (DEG) using the Kyoto Encyclopedia of Genes and Genomes (KEGG) pathway showed that these DEGs were enriched in biological processes related to cell growth and death (Supplementary Fig. S2B). Specifically, 16 genes were cell cycle–related genes among these DEGs (**Fig. 4A**; $P < 0.05$). We selected several cell cycle–related genes for verification. As shown in **Fig. 4B**, qRT-PCR results showed that MYC, ORC6, CCNA2, CDK4, CDK7, and CDC14A were downregulated, whereas CDKN1A, RB1, and GADD45B were upregulated in ESRRB-knockout cells compared with those in control cells. However, MYC, ORC6, CCNA2,

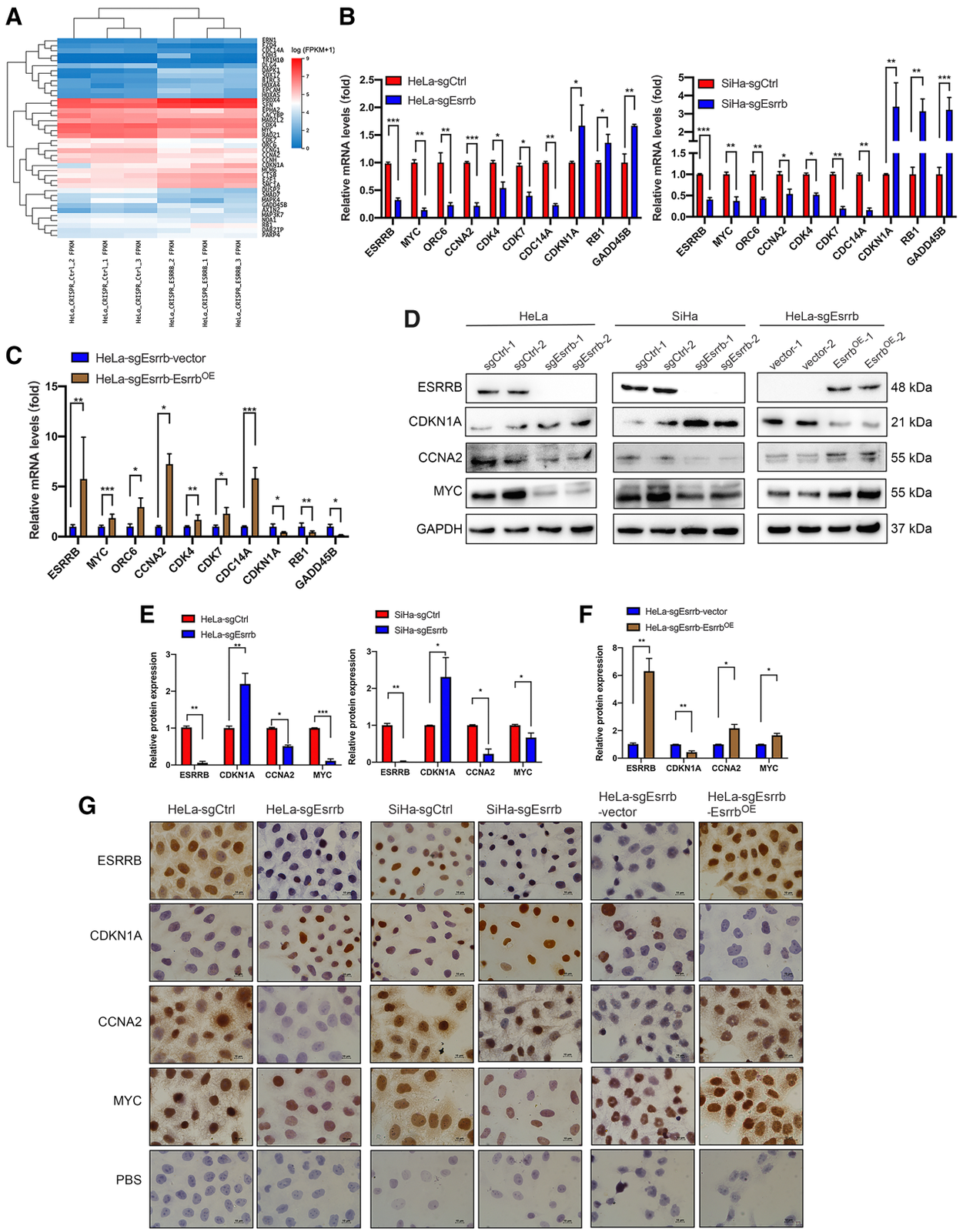
A
log (FPKM+1)
HeLa_CRISPR_Ctrl_2 FPKM
HeLa_CRISPR_Ctrl_1 FPKM
HeLa_CRISPR_Ctrl_3 FPKM
HeLa_CRISPR_ESRRB_2 FPKM
HeLa_CRISPR_ESRRB_1 FPKM
HeLa_CRISPR_ESRRB_3 FPKM
B
HeLa-sgCtrl
HeLa-sgEsrrb
SiHa-sgCtrl
SiHa-sgEsrrb
Relative mRNA levels (fold)
ESRRB
MYC
ORC6
CCNA2
CDK4
CDK7
CDC14A
CDKN1A
RB1
GADD45B
C
HeLa-sgEsrrb-vector
HeLa-sgEsrrb-EsrrbOE
Relative mRNA levels (fold)
D
HeLa
SiHa
HeLa-sgEsrrb
sgCtrl-1
sgCtrl-2
sgEsrrb-1
sgEsrrb-2
vector-1
vector-2
EsrrbOE-1
EsrrbOE-2
ESRRB
CDKN1A
CCNA2
MYC
GAPDH
48 kDa
21 kDa
55 kDa
55 kDa
37 kDa
E
HeLa-sgCtrl
HeLa-sgEsrrb
SiHa-sgCtrl
SiHa-sgEsrrb
Relative protein expression
ESRRB
CDKN1A
CCNA2
MYC
F
HeLa-sgEsrrb-vector
HeLa-sgEsrrb-EsrrbOE
Relative protein expression
G
HeLa-sgCtrl
HeLa-sgEsrrb
SiHa-sgCtrl
SiHa-sgEsrrb
HeLa-sgEsrrb -vector
HeLa-sgEsrrb -EsrrbOE
ESRRB
CDKN1A
CCNA2
MYC
PBS

CDK4, CDK7, and CDC14A were upregulated, whereas CDKN1A, RB1, and GADD45B were downregulated in HeLa-sgEsrrb-Esrrb^{OE} compared with those in control cells (**Fig. 4C**, $P < 0.05$). In addition, Western blotting (**Fig. 4D** and **E**, $P < 0.05$) showed that the expression of CDKN1A was increased whereas the expression of CCNA2 and MYC was decreased in ESRRB-knockout cells compared with those in control cells. Conversely, the expression of CDKN1A was decreased, whereas the expression of CCNA2 and MYC was increased in HeLa-sgEsrrb-Esrrb^{OE} compared with those in control cells (**Fig. 4D** and **F**, $P < 0.05$). Then, we performed immunocytochemistry (ICC) staining (**Fig. 4G**) in ESRRB-modified cells and IHC staining and score analysis (Supplementary Fig. S2C, $P < 0.05$) in tumor xenograft tissues to examine the expression of CDKN1A, CCNA2, and MYC. We also provided wide-field images of ICC (Supplementary Fig. S3). The results also showed that the expression of CDKN1A increased, whereas the expression of CCNA2 and MYC decreased in HeLa-sgEsrrb cells and tumor xenograft tissues derived from HeLa-sgEsrrb. However, the expression of CDKN1A decreased, whereas the expression of CCNA2 and MYC increased in HeLa-sgEsrrb-Esrrb^{OE} cells and tumor xenograft tissues derived from HeLa-sgEsrrb-Esrrb^{OE} (Supplementary Fig. S2C, $P < 0.05$). In summary, ESRRB promotes the development and progression of cervical cancer by upregulating the genes promoting cell-cycle progression and downregulating the genes inhibiting cell-cycle progression.

ESRRB regulates the expression of cell cycle–related molecules by inhibiting the TGFβ signaling pathway via inhibition of SMAD2/3 phosphorylation and nuclear translocation

Next, KEGG enrichment analysis of sequencing data showed that DEGs were involved in multiple pathways. Among them, the TGFβ signaling pathway has been shown to play an important role in cancer (**Fig. 5A**; ref. 23). Previous studies have reported that phosphorylation of the SMAD2 C-terminus at the Ser-465/467 site and the SMAD3 C-terminus at the Ser-423/425 site can assemble into a trimeric complex with SMAD4, and then the complex can translocate to the nucleus, where the complex regulates the expression of downstream genes of the TGFβ pathway, including *CDKN1A, CCNA2,* and *MYC* (24). First, we analyzed SMAD2, SMAD3, and SMAD4 expression at the transcriptional level by qRT-PCR. The results showed that the expression of SMAD2, SMAD3, and SMAD4 was not significantly different between ESRRB-modified cells and their control cells (**Fig. 5B**). To verify whether the expression of CDKN1A, CCNA2, and MYC was affected by changes in the accumulation of the pSMAD2$^{Ser465/467}$/pSMAD3$^{Ser423/425}$/SMAD4 complex in nucleus, we performed nuclear and cytoplasmic fractionation assays on ESRRB-modified cells and their control cells. Western blotting showed that ESRRB deficiency in HeLa and SiHa cells led to increased expression of pSMAD2$^{Ser465/467}$, pSMAD3$^{Ser423/425}$, and SMAD4 in the nucleus but decreased expression of total SMAD2, SMAD3, and SMAD4 in the cytoplasm (**Fig. 5C**–**E**, $P < 0.05$). At the same time, ESRRB deficiency in HeLa and SiHa cells also increased the cytoplasmic pSMAD2$^{Ser465/467}$ and pSMAD3$^{Ser423/425}$ levels (**Fig. 5C** and **E**, $P < 0.05$). However, overexpression of ESRRB in HeLa-sgEsrrb led to decreased expression of pSMAD2$^{Ser465/467}$, pSMAD3 $^{Ser423/425}$, and SMAD4 in the nucleus but increased expression of total SMAD2, SMAD3, and SMAD4 in the cytoplasm (**Fig. 5C**, F, and G, $P < 0.05$). Additionally, overexpressing ESRRB in HeLa-sgEsrrb decreased cytoplasmic pSMAD2$^{Ser465/467}$ and pSMAD3$^{Ser423/425}$ levels (**Fig. 5C** and **G**, $P < 0.05$). In addition, ICC staining showed that the staining of pSMAD2$^{Ser465/467}$, pSMAD3 $^{Ser423/425}$, and SMAD4 in the nucleus of ESRRB-knockout cells was significantly enhanced (**Fig. 5H**), whereas the staining of pSMAD2$^{Ser465/467}$, pSMAD3$^{Ser423/425}$, and SMAD4 in the nucleus of HeLa-sgEsrrb overexpressing ESRRB was weakened (**Fig. 5I**). We also provided wide-field images of ICC (Supplementary Fig. S3). All these results indicate that ESRRB affects the activity of SMAD2 and SMAD3 through posttranslational regulation rather than transcriptional regulation. ESRRB leads to reduced phosphorylation of SMAD2 and SMAD3 in the cytoplasm, resulting in reduced formation of the pSMAD2$^{Ser465/467}$/pSMAD3$^{Ser423/425}$/SMAD4 complex and reduces the accumulation of this complex in the nucleus, which inhibits the effect of the pSMAD2$^{Ser465/467}$/pSMAD3$^{Ser423/425}$/SMAD4 complex on the downstream genes of the TGFβ pathway.

To investigate whether the nuclear translocation of the pSMAD2$^{Ser465/467}$/pSMAD3$^{Ser423/425}$/SMAD4 complex transcriptionally regulates the downstream genes of the TGFβ pathway, we constructed an SBE luciferase reporter plasmid containing the binding site of the pSMAD2$^{Ser465/467}$/pSMAD3$^{Ser423/425}$/SMAD4 complex. The activity of the SBE plasmid was increased by 5.27 ± 1.69-fold in HeLa-sgEsrrb compared with that in HeLa-sgCtrl (**Fig. 5J**, $P < 0.05$). Likewise, the activity of the SBE plasmid was increased by 6.33 ± 2.09-fold in SiHa-sgEsrrb compared with that in SiHa-sgCtrl (**Fig. 5K**, $P < 0.05$). However, the activity of the SBE plasmid was decreased by 2 ± 0.14-fold in HeLa-sgEsrrb-Esrrb^{OE} compared with that in HeLa-sgEsrrb-vector (**Fig. 5L**, $P < 0.01$). In conclusion, ESRRB inhibits the transcriptional activity of the pSMAD2$^{Ser465/467}$/pSMAD3$^{Ser423/425}$/SMAD4 complex by inhibiting the phosphorylation of SMAD2/3 and the formation of the pSMAD2$^{Ser465/467}$/pSMAD3$^{Ser423/425}$/SMAD4 complex.

ESRRB transactivates *SMAD7* to inhibit the TGFβ signaling pathway, which promotes MYC expression, and MYC not only transactivates *ESRRB* but also upregulates SMAD7 expression

SMAD7 has been shown to prevent the phosphorylation of SMAD2/SMAD3 and translocation of the pSMAD2$^{Ser465/467}$/pSMAD3$^{Ser423/425}$/SMAD4 complex to the nucleus (25). Analysis of transcriptome sequencing data showed that SMAD7 was downregulated in HeLa-sgEsrrb cells (**Fig. 4A**). Furthermore, we analyzed the overall survival (OS) probability in 304 patients with cervical cancer in The Cancer Genome Atlas (TCGA) RNA database by the

Figure 4.

ESRRB facilitates cervical cancer cell proliferation by regulating cell cycle–related proteins. **A,** Expression heat map of significantly differentially expressed transcripts following ESRRB knockout. Red, genes that were upregulated compared with the control cells; blue, genes that were downregulated compared with the control cells (biological replicates = 3 per group). **B** and **C,** qRT-PCR analyzes the relative expression of a number of genes related to the cell cycle in ESRRB-knockout cells compared with their control cells (**B**), as well as in HeLa-sgEsrrb-Esrrb^{OE} cells compared with its control cells (**C**). **D–G,** Western blotting (**D–F**) and ICC (**G**; scale bar, 10 μm) detected CDKN1A, MYC, and CCNA2 expression in the ESRRB-modified cells and their control cells. The Western blotting bands were quantified and normalized to GAPDH. Representative images are shown. Wide-field of **G** is in Supplementary Fig. S3. All data, mean ± SD. Student *t* test was used for statistical analysis. *, $P < 0.05$; **, $P < 0.01$; ***, $P < 0.001$. All data represent at least three independent experiments.

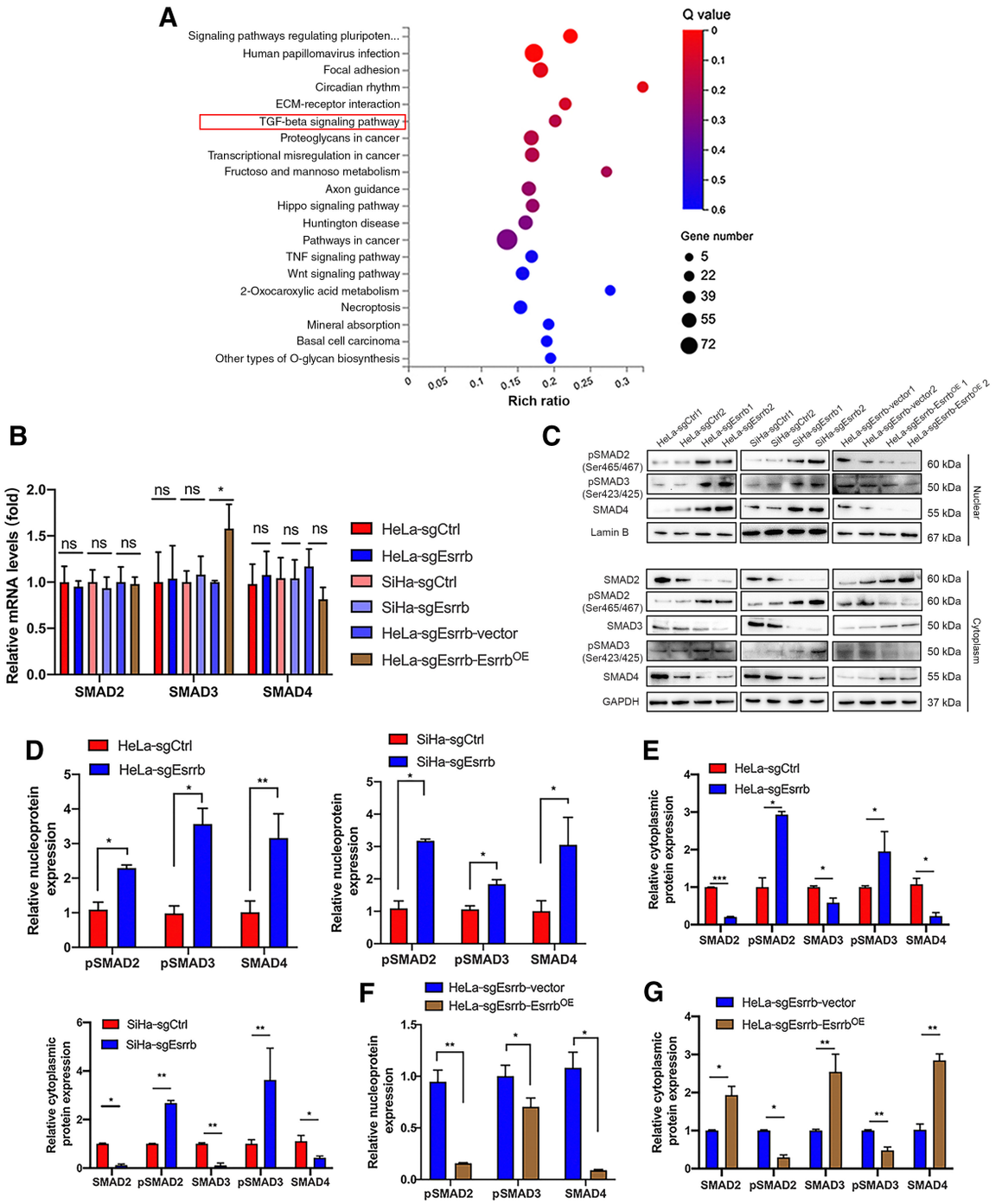

Figure 5.

ESRRB regulates the expression of cell cycle–related molecules by inhibiting the TGFβ signaling pathway via inhibition of SMAD2/3 phosphorylation and nuclear translocation. **A,** Enrichment analysis of the KEGG pathway after ESRRB knockout showed that the DEGs are enriched in the TGFβ pathway. **B,** qRT-PCR was used to detect the expression of SMAD2, SMAD3, and SMAD4 at the mRNA level. **C–G,** Nuclear-Cytosol Extraction Kit was used to perform cell separation. SMAD2, SMAD3, and SMAD4 proteins from the cytoplasm were detected by Western blotting. pSMAD2$^{Ser465/467}$ and pSMAD3$^{Ser423/425}$ proteins from the nucleus and cytoplasm were also detected by Western blotting, respectively (**C**). The Western blotting bands were quantified and normalized to GAPDH to indicate relative nuclear or cytoplasmic expression in ESRRB-knockout cells compared with their control cells (**D** and **E**), as well as in HeLa-sgEsrrb-Esrrb^{OE} compared with its control cells (**F** and **G**). (*Continued on the following page.*)

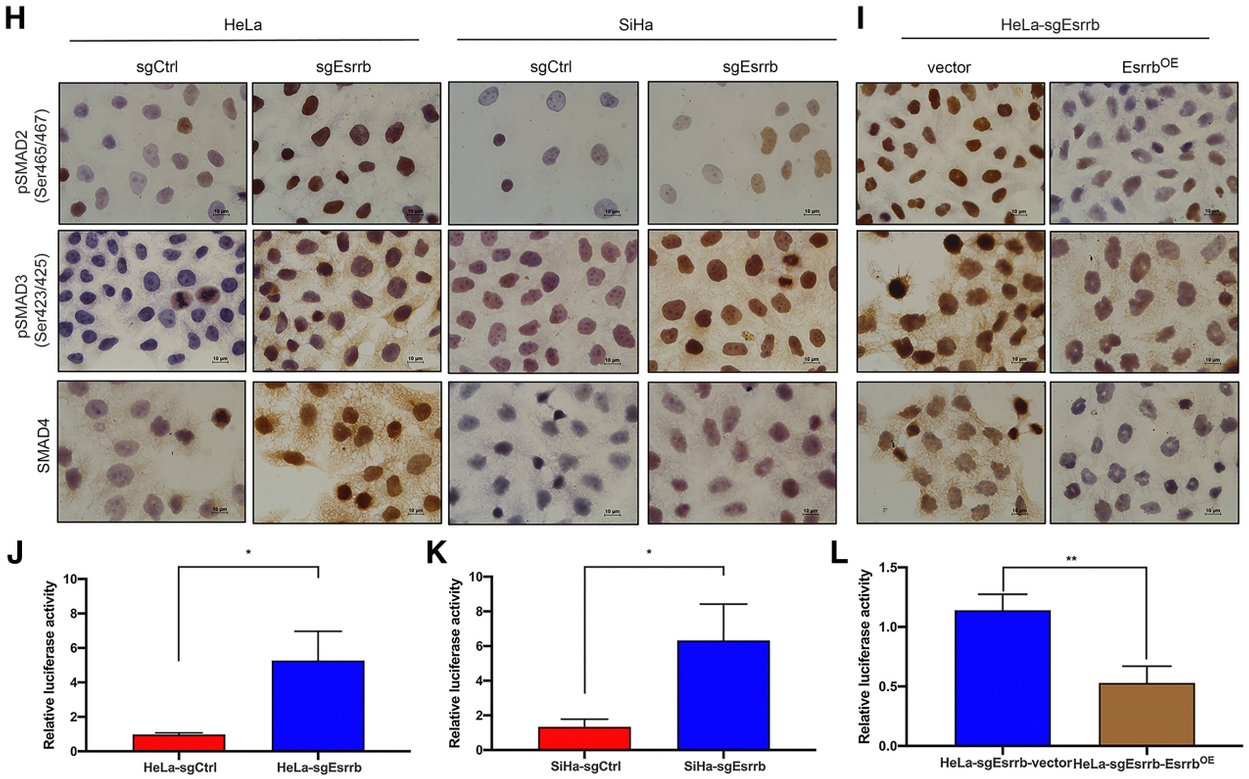

Figure 5.

(*Continued.*) **H** and **I,** Representative images of nuclear translocation of pSMAD2$^{Ser465/467}$, pSMAD3$^{Ser423/425}$, and SMAD4 in indicated cells by ICC. Scale bar, 10 μm. Wide-field view is in Supplementary Fig S3. **J** and **K,** ESRRB-knockout cells and their control cells were transfected with SBE luciferase reporter for 48 hours and the cell lysates were used to measure luciferase activity. **L,** The SBE luciferase reporter was also transfected into HeLa-sgEsrrb-Esrrb^{OE} and its control cells to measure SBE luciferase activity. Data are shown as relative luciferase activity (pGL3-SBE4-Luc activity/pRL-SV40-luc activity). All data, mean ± SD. Student *t* test was used for statistical analysis. *, $P < 0.05$; **, $P < 0.01$; ***, $P < 0.001$; ns, nonsignificant. All data are representative of three independent experiments.

Kaplan–Meier plotter (http://kmplot.com/analysis/). The results demonstrated that the level of SMAD7 increased, and the probability of cervical cancer patients' OS decreased with statistical significance (Supplementary Fig. S4A, $P < 0.05$). It proved that SMAD7 is a poor prognostic factor in cervical cancer. Our data showed that ESRRB can inhibit the phosphorylation of SMAD2 and SMAD3, thus reducing its formation of a complex with SMAD4 and reducing translocation of this complex to the nucleus, leading to upregulated MYC expression. Therefore, to verify that SMAD7 is involved in ESRRB-mediated inhibition of pSMAD2$^{Ser465/467}$/pSMAD3$^{Ser423/425}$/SMAD4 complex formation, the expression of SMAD7 at both the mRNA and protein levels was examined. In ESRRB-knockout cells, the expression of SMAD7 was decreased compared with control cells (**Fig. 6A**, **B**, and **C**, $P < 0.05$), whereas the expression of SMAD7 in HeLa-sgEsrrb-Esrrb^{OE} was increased compared with that in control cells (**Fig. 6A**, **C**, and **D**, $P < 0.05$). The expression of SMAD7 was also detected in ESRRB-modified cells by ICC (Supplementary Fig. S4B). We also provided wide-field images of SMAD7 ICC staining (Supplementary Fig. S3). Furthermore, the expression of SMAD7 in tumor xenograft tissues derived from ESRRB-knockout cells was significantly decreased compared with that in tumor xenograft tissues derived from their control cells (Supplementary Fig. S4C–S4E, $P < 0.01$). Conversely, the expression of SMAD7 in tumor xenograft tissues derived from HeLa-sgEsrrb-Esrrb^{OE} cells was increased compared with that in tumor xenograft tissues derived from HeLa-sgEsrrb-vector cells (Supplementary Fig. S4F, $P < 0.05$). To verify the dynamic effect of ESRRB on SMAD7 expression, CRISPR/Cas9 plasmids targeting ESRRB at different concentrations and control plasmids were transiently transfected into HeLa and 293T cells. The results of qRT-PCR and Western blotting showed that the expression of SMAD7 decreased, accompanied by a decrease in ESRRB expression, suggesting that the expression of SMAD7 was regulated by ESRRB in a dose-dependent manner (Supplementary Fig. S4G, $P < 0.05$). In addition, 4 μg of CRISPR/Cas9 plasmids targeting ESRRB and control plasmids was transiently transfected into 293T cells, and then the cells transfected with CRISPR/Cas9 plasmids were collected at different times. The results of qRT-PCR and Western blotting showed that the expression of SMAD7 decreased with extended transfection time of the CRISPR/Cas9 plasmids, suggesting that the expression of SMAD7 was regulated by ESRRB in a time-dependent manner (Supplementary Fig. S4H, $P < 0.05$). All these results suggest that ESRRB upregulates SMAD7 expression.

Using the JASPAR database (https://jaspar.genereg.net/), the binding site of ESRRB was found 5′-AAGGTCA-'3, and this motif can be found in the promoter of *SMAD7* (**Fig. 6E**). Thus, SMAD7 may be a potential target of ESRRB. To clarify whether ESRRB transactivated *SMAD7*, the full-length [−2,000 to +500 bp, relative to the transcription start site (TSS), P1] and truncated fragments (P2-P7) of the *SMAD7* promoter were cloned into a pGL3-Basic luciferase plasmid. The results indicated that the luciferase activity of P1-P6 was decreased

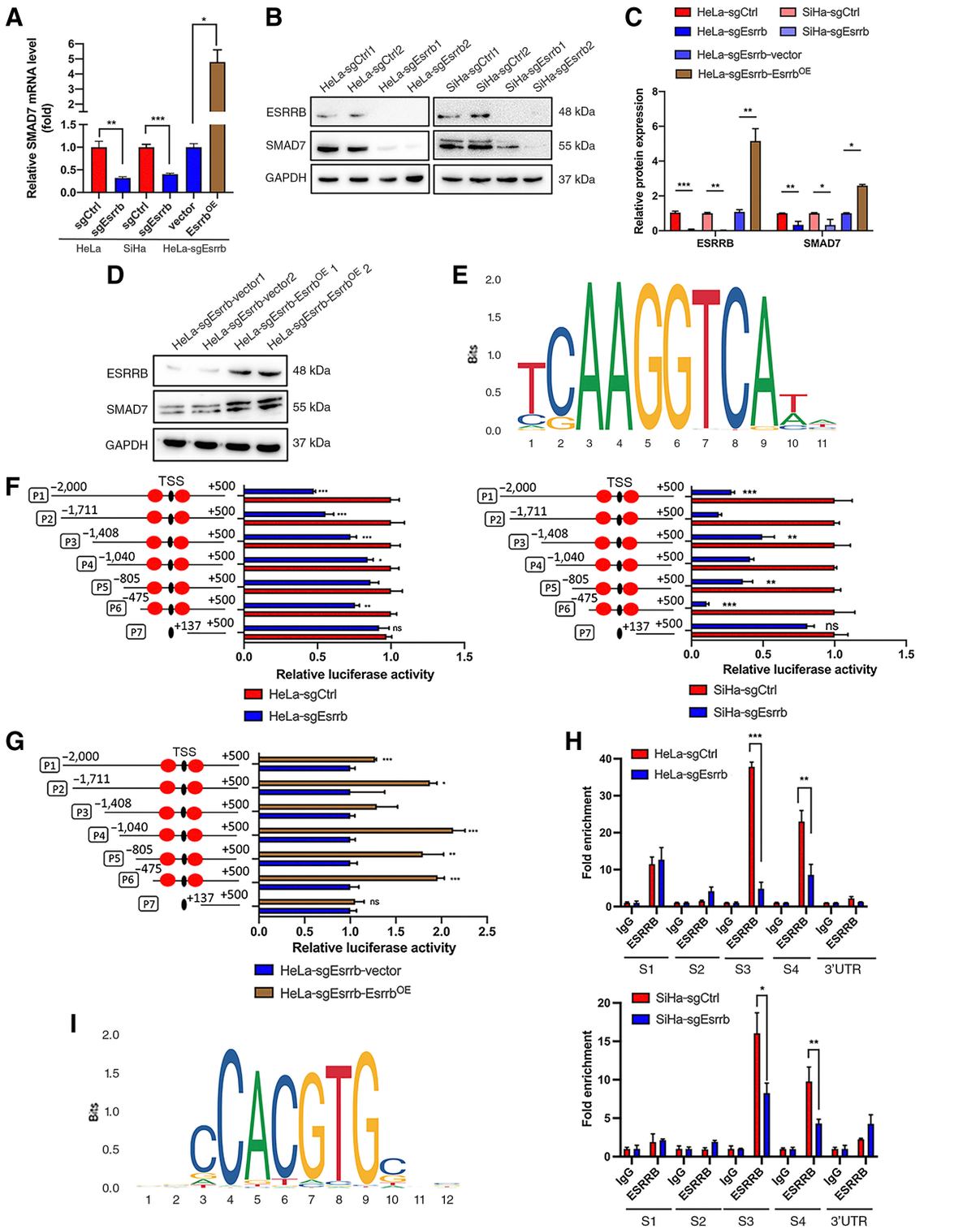

Figure 6.

ESRRB transactivates SMAD7 to inhibit the TGFβ signaling pathway, which promotes MYC expression, and MYC not only transactivates ESRRB but also upregulates SMAD7 expression. **A–D,** qRT-PCR (**A**) and Western blotting (**B–D**) verified the SMAD7 expression in ESRRB-modified cells and their control cells. The Western blotting bands were quantified and normalized to GAPDH. **E,** Schematic diagram of ESRRB-binding motif. **F** and **G,** Luciferase reporter plasmids containing various lengths of the promoter region of SMAD7 were transiently transfected into ESRRB-modified HeLa, SiHa (**F**), and HeLa-sgEsrrb (**G**) cells and their control cells. The ratio of the Luc/*Renilla* activity is shown as mean ± SD of three independent assays. The red dots represent the approximate location of the ESRRB binding site. **H,** HeLa-sgEsrrb, SiHa-sgEsrrb, and their control cells were subjected to ChIP-qPCR assays using anti-ESRRB and anti-IgG, respectively. Data were normalized by 2% input. Fold enrichment is shown as mean ± SD of three independent assays. S1, S2, S3, S4, and 3′UTR represent different primers to amplify different fragments of the promoter. **I,** Schematic diagram of MYC-binding motif. (*Continued on the following page.*)

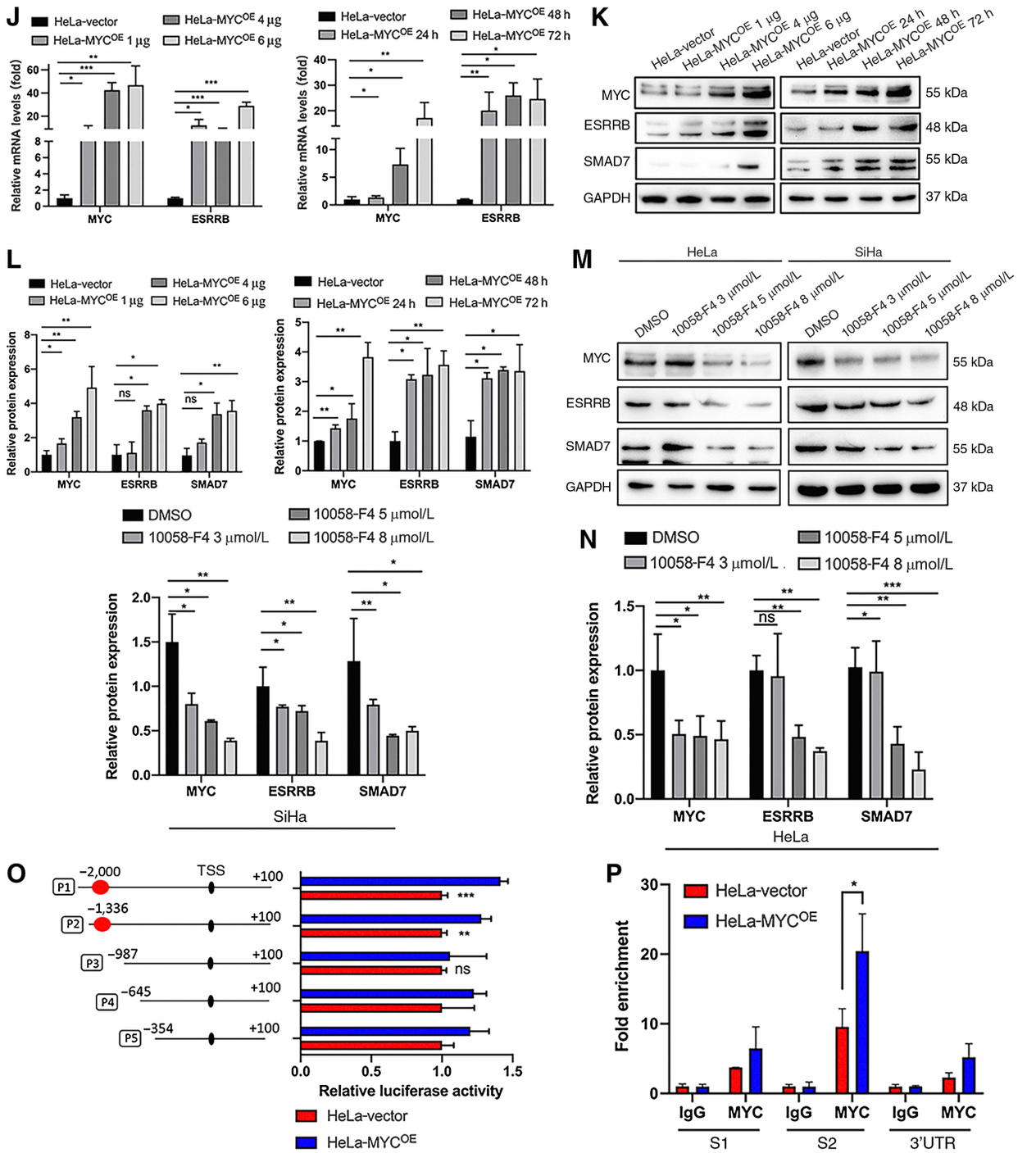

Figure 6.

(*Continued.*) **J–L,** The expression of MYC and ESRRB was detected by qRT-PCR (**J**) and the expression of MYC, ESRRB, and SMAD7 was detected by Western blotting in HeLa-MYC^{OE} cells and its control cells (**K** and **L**). **M** and **N,** The expression levels of MYC, ESRRB, and SMAD7 in HeLa and SiHa cells treated with 10058-F4 or DMSO were detected by Western blotting. The Western blotting bands were quantified and normalized to GAPDH. **O,** Luciferase assays assessing the promoter activity of ESRRB were measured in HeLa-MYC^{OE} and HeLa-vector. The red dots represent the approximate location of the ESRRB binding site. **P,** HeLa-MYC^{OE} and HeLa-vector were subjected to ChIP-qPCR assay using anti-MYC antibody. S1 and S2 represent different regions of the ESRRB promoter (−1336 bp to − 987 bp). Data were normalized by 2% input. Fold enrichment is presented as mean ± SD of three different experiments. The transcription start sites are indicated as TSS. S1, S2, and 3′UTR represent different primers to amplify different fragments of the promoter. Student *t* test was used for statistical analysis. *, $P < 0.05$; **, $P < 0.01$; ***, $P < 0.001$; ns, nonsignificant. All data are representative of three independent experiments and their control cells. (**E** and **I,** Created with JASPAR 2022.)

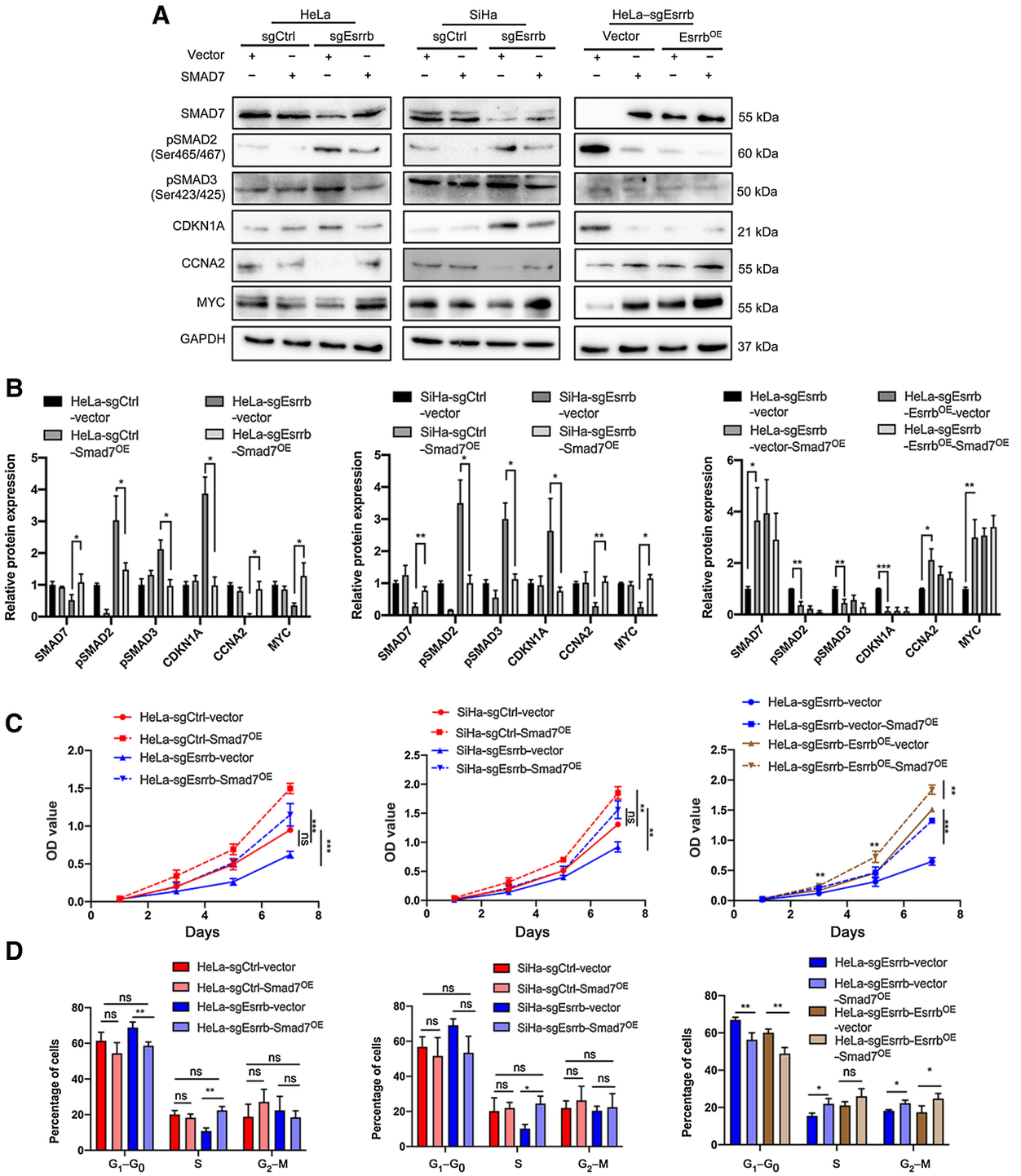

Figure 7.

SMAD7 overexpression or treatment with SB525334 upregulates MYC and ESRRB and rescues the proliferative ability of ESRRB-knockout cervical cancer cells. **A** and **B,** The protein levels of SMAD7, pSMAD2$^{Ser465/467}$, pSMAD3$^{Ser423/425}$, CDKN1A, CCNA2, MYC in HeLa-sgEsrrb (left), SiHa-sgEsrrb (middle), HeLa-sgEsrrb-vector (right), and their control cells were detected by Western blotting. The Western blotting bands were quantified and normalized to GAPDH. **C** and **D,** CCK8 assay (**C**) and cell cycle (**D**) showed the proliferative capabilities of ESRRB-modified cells after overexpressing SMAD7. (*Continued on the following page.*)

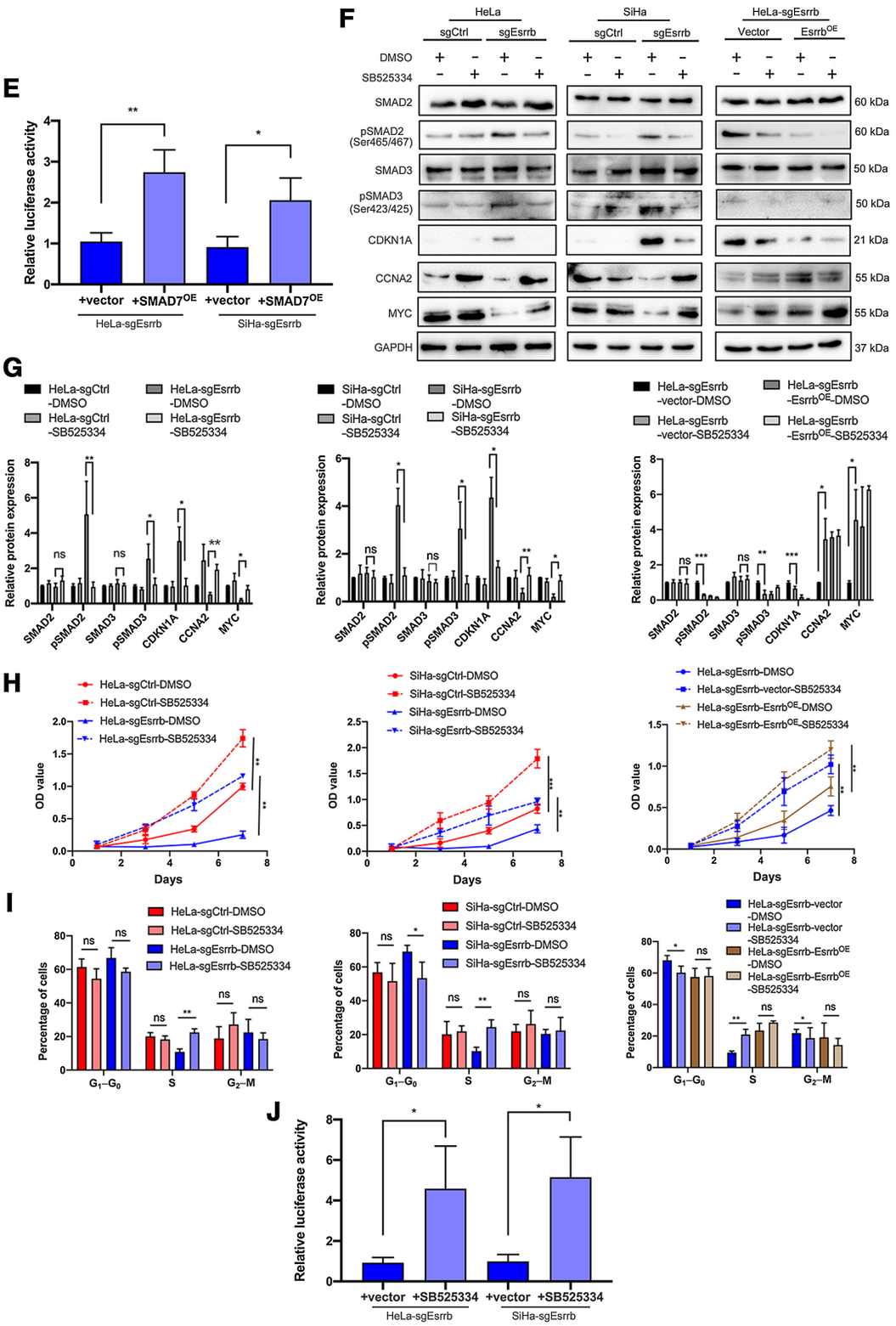

Figure 7.

(*Continued.*) **E,** The activity of the ESRRB promoter was detected after overexpressing SMAD7. Data are shown as relative luciferase activity. **F** and **G,** The HeLa-sgEsrrb (left), SiHa-sgEsrrb (middle), and HeLa-sgEsrrb-vector (right) were respectively treated with SB525334 and DMSO. Their control cells also were respectively treated with SB525334 and DMSO. The protein levels of SMAD2, pSMAD2$^{Ser465/467}$, SMAD3, pSMAD3$^{Ser423/425}$, CDKN1A, CCNA2, and MYC were detected by Western blotting. The Western blotting bands were quantified and normalized to GAPDH. **H** and **I,** CCK8 assay (**H**) and cell cycle (**I**) showed the proliferative capabilities of ESRRB-modified cells after treatment with SB525334. **J,** The activity of ESRRB promoter was detected after treatment with SB525334. Data are shown as relative luciferase activity. All data, mean ± SD. Student *t* test was used for statistical analysis. *, $P < 0.05$; **, $P < 0.01$; ***, $P < 0.001$; ns, nonsignificant. All data are representative of three independent experiments.

in ESRRB-knockout cells compared with that in control cells (**Fig. 6F**, $P < 0.05$), whereas the luciferase activity of P7 showed no differences between ESRRB-knockout cells and control cells (**Fig. 6F**). The luciferase activity of P1–P6 in HeLa-sgEsrrb-Esrrb^{OE} was increased compared with that in control cells (**Fig. 6G**, $P < 0.05$), whereas P7 did not change (**Fig. 6G**). In addition, the luciferase activity of P1-P6 in 293T-Esrrb^{OE} cells was also increased compared with that in control cells (Supplementary Fig. S5A, $P < 0.05$). This suggests that the regulatory site of ESRRB is located at −475 to +137 bp of the *SMAD7* promoter. To further determine whether ESRRB can directly bind to −475 to +137 bp of the *SMAD7* promoter, a ChIP-qPCR assay was performed in ESRRB-knockout cells using an anti-ESRRB antibody and IgG (negative control). Four pairs of primers were designed to amplify four (S1–S4) fragments of −475 to +137 bp of the *SMAD7* promoter (Supplementary Fig. S5B). The results showed that S3 and S4 fragments (S3: −185 to −87 bp; S4: −19 to +129 bp) were significantly enriched in HeLa-sgCtrl and SiHa-sgCtrl cells after immunoprecipitation with ESRRB antibody (**Fig. 6H**, $P < 0.05$). Amplification of the *SMAD7* promoter (S1-S4) using IgG antibody as a negative control did not enrich ESRRB-knockout cells and their control cells (**Fig. 6H**). Collectively, our data suggest that ESRRB can directly bind to the *SMAD7* promoter.

To the best of our knowledge, few studies have elucidated how ESRRB expression is regulated. Thus, the UCSC Genome Browser database (http://genome.ucsc.edu/) was used to predict the transcription factors that can bind to the *ESRRB* promoter. MYC, a downstream molecule of the TGFβ pathway, was found to bind to the *ESRRB* promoter. The JASPAR database revealed that the binding site of MYC is 5′-CCACGTG-'3, and the promoter of *ESRRB* indeed contains putative MYC-binding sites (**Fig. 6I**). Therefore, we constructed an MYC-overexpression plasmid and transfected it into HeLa cells. The results showed that overexpressing MYC upregulated ESRRB and SMAD7 expression in a time and dose-dependent manner (**Fig. 6J**, **K**, and **L**, $P < 0.05$). Conversely, 10058-F4, a MYC inhibitor, inhibited ESRRB and SMAD7 expression in a dose-dependent manner in HeLa and SiHa cells (**Fig. 6M** and **N**, $P < 0.05$). To assess whether MYC promoted ESRRB expression by transactivating *ESRRB*, different concentrations of MYC overexpression plasmids were transfected into HeLa cells and different concentrations of MYC inhibitors 10058-F4 were added into SiHa cells. Then, these cells were cotransfected with *ESRRB* promoter-reporter plasmid. The result demonstrates that MYC transactivates *ESRRB* (Supplementary Fig. S5C, $P < 0.05$). To further explore the site of MYC transactivating *ESRRB* promoter, full-length (−2,000 to +100 bp, relative to the TSS, P1) and truncated fragments (P2–P5) of the *ESRRB* promoter were cloned into a pGL3-Basic luciferase plasmid. The luciferase activity of P1 and P2 in HeLa-MYC^{OE} cells was significantly higher than that in HeLa-vector cells (**Fig. 6O**, $P < 0.01$). However, the luciferase activity of other truncated fragments showed no significant differences between HeLa-MYC^{OE} cells and HeLa-vector cells, suggesting that MYC transactivated *ESRRB* by binding to the −1,336 to −987 bp region of the *ESRRB* promoter. In addition, to further determine whether the MYC can directly bind to the −1,336 to −987 bp region of the *ESRRB* promoter, ChIP-qPCR was performed. Two pairs of primers were designed to amplify two (S1 and S2) fragments of the −1,336 to −987 bp region of the *ESRRB* promoter (Supplementary Fig. S5D). The results showed that the S2 fragment (−1,177 bp to −987 bp) was significantly enriched in HeLa-MYC^{OE} cells after immunoprecipitation with MYC antibody (**Fig. 6P**, $P < 0.05$). Thus, these data suggest that MYC transactivates *ESRRB* by directly binding to its promoter and upregulates SMAD7 expression.

SMAD7 overexpression or treatment with SB525334 upregulates MYC and the promoter activity of *ESRRB* and rescues the proliferative ability of ESRRB-knockout cervical cancer cells

To further confirm that ESRRB transactivates *SMAD7* to promote the proliferation of cervical cancer cells, we transiently transfected SMAD7 plasmids and control plasmids into ESRRB-knockout cells, respectively. In addition, the control cells corresponding to ESRRB-knockout cells were also transfected with SMAD7 plasmids and control plasmids, respectively. Our data showed that ectopic expression of SMAD7 in ESRRB-knockout cells suppressed the pSMAD2$^{Ser465/467}$ and pSMAD3$^{Ser423/425}$ levels, downregulated the expression of CDKN1A and upregulated the expression of CCNA2 and MYC compared with the control plasmids transfected in ESRRB-knockout cells (**Fig. 7A** and **B**, $P < 0.05$). Simultaneously, the proliferative capacity of ESRRB-knockout cells transfected with the SMAD7 plasmids was much higher than that of ESRRB-knockout cells transfected with the control plasmids (**Fig. 7C** and **D**, $P < 0.05$). Furthermore, overexpressing SMAD7 dramatically increased *ESRRB* promoter activity and suppressed SBE reporter activity in ESRRB-knockout cells (**Fig. 7E**; Supplementary Fig. S5E, $P < 0.05$).

In addition, SB525334 inhibits the phosphorylation of TGFβ type I receptor (TβRI), thereby inhibiting the phosphorylation of SMAD2 and SMAD3 (26). Our data showed that ESRRB-knockout cells treated with SB525334 for 24 hours at a concentration of 2 μmol/L suppressed the pSMAD2$^{Ser465/467}$ and pSMAD3$^{Ser423/425}$ protein levels, downregulated the expression of CDKN1A and upregulated the expression of CCNA2 and MYC compared with those cells treated with dimethyl sulfoxide (DMSO; **Fig. 7F** and **G**, $P < 0.05$). Moreover, the proliferative capacity of ESRRB-knockout cells treated with SB525334 was much higher than that of cells treated with DMSO (**Fig. 7H** and **I**, $P < 0.05$). The addition of SB525334 to ESRRB-knockout cells also increased *ESRRB* promoter activity and suppressed the activity of the SBE reporter (**Fig. 7J**; Supplementary Fig. S5F, $P < 0.05$).

All of the above results indicated that overexpressing SMAD7 and SB525334 rescued the proliferative capacity caused by the loss of ESRRB and upregulate MYC by inhibiting TGFβ pathway activity, thereby transactivating *ESRRB*. Our data have shown that ESRRB transactivated *SMAD7* and upregulated MYC expression. MYC transactivated *ESRRB* and upregulated SMAD7 expression. Thus, ESRRB, SMAD7, and MYC can form an ESRRB/SMAD7/MYC–positive feedback loop in cervical cancer.

Clinical correlation between ESRRB and TGFβ signaling-related genes in human cervical cancer tissues

Based on the mechanism we explored, we further investigated the clinical correlation between ESRRB and TGFβ signaling-related genes in 30 cervical cancer samples (**Fig. 8A**). ESRRB was negatively correlated with the expression of pSMAD2$^{Ser465/467}$, pSMAD3$^{Ser423/425}$, and CDKN1A (**Fig. 8B–D**). ESRRB was positively correlated with the expression of SMAD7, CCNA2, and MYC (**Fig. 8E–G**). These results further support a positive feedback loop between ESRRB and SMAD7 and MYC in cervical cancer. In addition, the low expression of CDKN1A and the high expression of CCNA2 and MYC were all related to poor prognosis of cervical cancer (Supplementary Fig. S5G).

Altogether, our data first suggest that upregulation of ESRRB is associated with the progression of human cervical cancer. ESRRB transactivates *SMAD7* through directly binding to its promoter, thereby inhibiting the phosphorylation of SMAD2 and SMAD3. The insufficient phosphorylation of SMAD2 and SMAD3 cannot form a complex with SMAD4, thus inhibiting the nuclear translocation of the

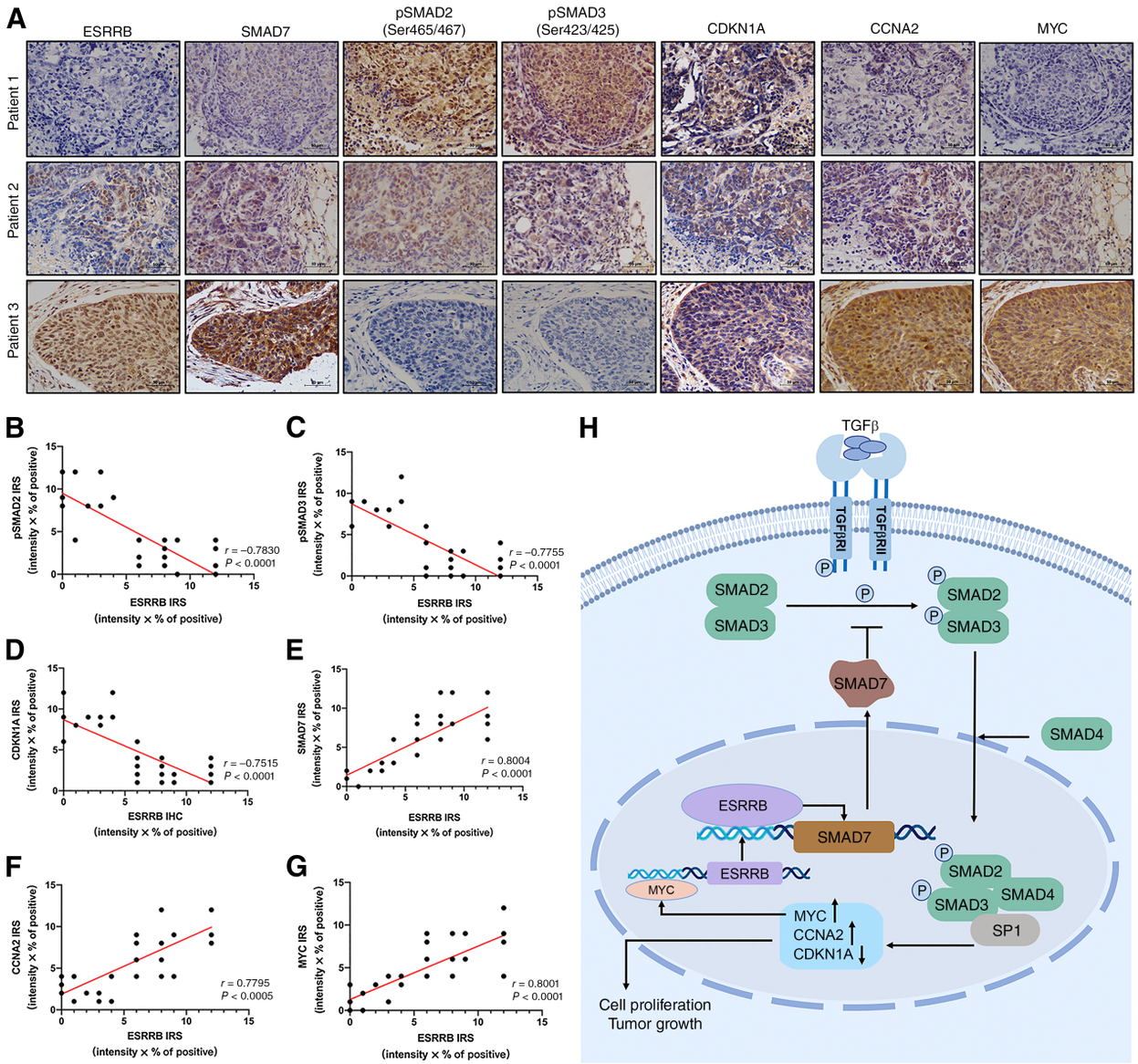

Figure 8.

Clinical correlation between ESRRB and TGFβ signaling-related genes in human cervical cancer tissues. **A,** Representative immunostaining of ESRRB, SMAD7, pSMAD2$^{Ser465/467}$, pSMAD3$^{Ser423/425}$, CDKN1A, CCNA2, and MYC in CC tissues. Scale bar, 50 μm. **B–G,** The correlation between ESRRB and, pSMAD2$^{Ser465/467}$ (**B**), pSMAD3$^{Ser423/425}$ (**C**), CDKN1A (**D**), SMAD7 (**E**), CCNA2 (**F**), MYC (**G**) in 30 CC tissues. **H,** Schematic illustrates that ESRRB inhibits the phosphorylation of SMAD2, SMAD3, and the formation of trimers with SMAD4 through transactivating SMAD7, thus affecting the downstream target genes of the TGFβ signaling pathway, such as cell cycle–related molecules CDKN1A, CCNA2, and MYC due to the decreased translocation of pSMAD2$^{Ser465/467}$/pSMAD3$^{Ser423/425}$/SMAD4 into the nucleus. Finally, it promoted the proliferation ability of cervical cancer cells *in vitro* and tumorigenesis ability *in vivo*.

pSMAD2$^{Ser465/467}$/pSMAD3$^{Ser423/425}$/SMAD4 complex, and thus downregulating CDKN1A and upregulating CCNA2 and MYC. In turn, MYC transactivates *ESRRB* and upregulates SMAD7 level, which forms a positive feedback loop with ESRRB to promote cervical cancer proliferation (**Fig. 8H**).

Discussion

Globally, there were approximately 604,000 cases and 342,000 deaths from cervical cancer in 2020, suggesting a significant global burden of cervical cancer (1). Patients with metastatic or recurrent cervical cancer have limited responses to conventional therapies, thus requiring new forms of treatment (27). In recent years, the development of molecular-targeted and immunotherapeutic treatments has changed the treatment landscape for various cancers, especially non-small cell lung cancer and malignant melanoma. However, data on molecular-targeted treatment in cervical cancer lag behind other more common tumor types (28). Therefore, the molecular-targeted treatment of cervical cancer is an important problem. TCGA was used to comprehensively analyze the molecules involved in 228 cases of

cervical cancer. Many genes showed significant variation in cervical cancer, including *CASP8, HLAA, SHKBP1,* and *TGFBR2* (9). Therefore, the genes involved in the development of cervical cancer require further study.

It has also been reported that the expression of ESRRB in cancerous lesions is significantly lower than that in benign foci in breast and prostate cancer (29, 30). Pan-cancer analysis data for ESRRB showed low expression of ESRRB in most tumor tissues relative to normal tissues, but high expression in adenocarcinoma of the colon (CHOL), so the pattern of gene expression is different in different tumor types. Our data demonstrated that the expression of ESRRB in cervical cancer tissues was higher than that in normal cervical tissues (**Fig. 1**). IHC showed statistically significant differences in ESRRB expression between the NC group and the HSIL or CC group, whereas the differences between the HSIL and CC were not statistically significant, suggesting that ESRRB may play a role in the early stage of cervical carcinogenesis. IHC showed that ESRRB was mainly distributed in the nucleus, whereas there was also a small amount of ESRRB distributed in the cytoplasm. It has been proposed that some orphan receptors have nuclear export signals (NES) involved in their nuclear export to the cytoplasm (31). Therefore, ESRRB was located in the cytoplasm perhaps due to the existence of NES in its structure, although this speculation requires further exploration. To our knowledge, the present study is the first to reveal the expression of ESRRB in cervical cancer.

ESRRB has been reported to have antiproliferative properties in breast cancer cells (32). A study by Yu S and colleagues showed that ESRRB significantly suppressed the proliferation and tumorigenicity of prostate cancer cells (16). Our data clarified for the first time the relationship between ESRRB and the proliferative capacity of cervical cancer. ESRRB significantly promoted tumor growth *in vivo* (**Fig. 2**). *In vitro*, knocking out ESRRB significantly inhibited the cell proliferative capacity of HeLa and SiHa cells, and overexpressing ESRRB in ESRRB-knockout HeLa cells rescued the proliferative capacity. Flow cytometry analysis showed that ESRRB accelerated the G_1–S transition in cervical cancer cells, whereas apoptotic capacity showed no significant differences between ESRRB-modified cells and their control cells (**Fig. 3**). This suggests that ESRRB promotes proliferation by facilitating the cell cycle G_1–S transition, which is not related to apoptosis. Thus, our findings show that ESRRB is a tumor growth promoter in cervical cancer.

ESRRB has been reported to be involved in a variety of signaling pathways in tumors by interacting with different molecules. For example, ESRRB regulates the Hedgehog pathway (33). ESRRB plays an inhibitory role in the estrogen signaling pathway by reducing the mobility of ERα in breast cancer (34). The study by Yu S and colleagues highlighted that ESRRB transactivated *CDKN1A* in prostate cancer (16). Interestingly, our transcriptome sequencing data showed that CDKN1A was upregulated in HeLa-sgEsrrb compared with that in HeLa-sgCtrl (**Fig. 4A**). This may be due to the different mechanisms by which ESRRB regulated CDKN1A in different cancer types. Our data showed that CDKN1A expression was elevated in ESRRB-knockout cells, whereas CCNA2 and MYC expression was decreased. CDKN1A expression was decreased whereas CCNA2 and MYC were increased in HeLa-sgEsrrb-Esrrb^{OE} (**Fig. 4**). It has been documented that *CDKN1A, CCNA2,* and *MYC* are downstream genes of the TGFβ pathway (35–38). Many studies have focused on the coregulators and downstream genes of ESRRB. However, how ESRRB expression is regulated has not been widely reported. By using the UCSC database, MYC was identified as participating in the transcriptional regulation of ESRRB. As shown in **Fig. 6**, our data revealed for the first time that MYC transactivated *ESRRB* by directly binding to its promoter, which may be a mechanism of maintaining ESRRB expression.

Previous reports have identified several signaling pathways involved in the development of cervical cancer, including the TGFβ, NF-kB, and MAPK pathways (5, 39). It has also been reported that dysregulation of the TGFβ pathway is associated with HPV-related cervical cancer (40). The TGFβ pathway induces cell-cycle arrest in early cancer cells, suggesting that it plays an inhibitory role in tumor development. Interestingly, a study by Colak S and colleagues found that activation of the TGFβ pathway in advanced cancer cells can induce epithelial-to-mesenchymal transition (EMT; ref. 24). Thus, the role of the TGFβ pathway in cancer is complex. Our data showed for the first time that ESRRB inhibited the TGFβ pathway and thus promoted the development of cervical cancer. In detail, as shown in **Fig. 5**, ESRRB inhibited the activity of the TGFβ pathway via inhibiting the phosphorylation of SMAD2/3 in the cytoplasm, leading to reduced formation of a complex with SMAD4 and reduced translocation of the pSMAD2$^{Ser465/467}$/pSMAD3$^{Ser423/425}$/SMAD4 complex into the nucleus, where the complex regulated the downstream genes of the TGFβ pathway by directly binding to SBE. ESRRB has been demonstrated that inhibits SBE activity. Activated TGFβ binds to TβRII, which can recruit and phosphorylate TβRI at specific residues. Then, activated TβRI phosphorylates SMAD2 and SMAD3 at C-terminal serine residues. Subsequently, SB525334 rescued the decreased proliferative capacity, suppressed the pSMAD2$^{Ser465/467}$ and pSMAD3$^{Ser423/425}$ protein levels and downregulated the expression of CDKN1A and upregulated the expression of CCNA2 and MYC in ESRRB-knockout cells (**Fig. 7**). Previous studies have shown that the pSMAD2$^{Ser465/467}$/pSMAD3$^{Ser423/425}$/SMAD4 complex mediated downregulation of MYC and the upregulation of CDKN1A (36). Whether the complex regulates CCNA2 requires further study. CCNA2 expression is regulated by CDKN1A, so CCNA2 can also be regarded as downstream of the TGFβ pathway (37). However, the control cells corresponding to ESRRB-knockout cells with high levels of ESRRB had low activity of the TGFβ pathway. Thus, the use of SB525334 in these cells only exerted a marginal effect on cell proliferation. Additionally, negative correlations between ESRRB and pSMAD2$^{Ser465/467}$ or pSMAD3$^{Ser423/425}$ were found in clinical tissue samples from cervical cancer patients, supporting our findings in cell lines (**Fig. 8**).

Many molecules are involved in regulating TGFβ pathway activity. For example, SMAD6, SMAD7, and SnoN all take part in the inhibition of the TGFβ pathway (41, 42). SMAD7 competitively binds to activated TβRI and prevents SMAD2/3 phosphorylation (43). High SMAD7 levels are observed in several human malignancies. For instance, SMAD7 transcripts are increased in human pancreatic cancer compared with that in the normal pancreas (44). It has also been reported that gastric cancer patients have elevated levels of SMAD7 (45). The present study is the first report to reveal that ESRRB transactivates *SMAD7* and upregulates MYC in cervical cancer. The decreased proliferation of cervical cancer cells mediated by ESRRB deficiency was readily rescued by SMAD7 overexpression (**Fig. 7**). Overexpressing SMAD7 in ESRRB-knockout cells suppressed the pSMAD2$^{Ser465/467}$ and pSMAD3$^{Ser423/425}$ levels, downregulated the expression of CDKN1A, and upregulated the expression of CCNA2 and MYC. This suggests that SMAD7 is involved in the process by which ESRRB inhibits the TGFβ pathway. It has been shown that the association of SMAD7 with the Wnt/β-catenin pathway also plays an important role in the regulation of some transcription factors

(e.g., MYC; ref. 46). Therefore, the effect of SMAD7 on MYC may not only be regulated by the TGFβ pathway but also be related to the Wnt/β-catenin pathway, which needs to be further investigated. In summary, ESRRB transactivates *SMAD7* to upregulate MYC. MYC transactivates *ESRRB* and upregulates SMAD7. SMAD7 increased *ESRRB* promoter activity by upregulating MYC. Therefore, we propose for the first time the existence of a positive feedback loop of ESRRB/SMAD7/MYC in cervical cancer. Positive feedback loops reduce spurious cellular phenotype alterations and help stabilize and enforce the cell phenotype (47). Thus, the presence of the ESRRB/SMAD7/MYC-positive feedback loop may lead to persistent high expression of ESRRB and inactivation of the TGFβ pathway in cervical cancer. A clinical correlation analysis showed that ESRRB was positively correlated with SMAD7 and MYC. Kaplan-Meier analysis showed that the high expression of SMAD7 and MYC was associated with shorter OS (Figs. S4A and S5G, $P < 0.05$). These results support the conclusion that the ESRRB/SMAD7/MYC-positive feedback loop promotes the development and progression of cervical cancer.

Altogether, our study demonstrates that ESRRB inhibits the TGFβ pathway through transactivating *SMAD7*, which downregulates CDKN1A expression and upregulates CCNA2 and MYC expression. In turn, MYC transactivates *ESRRB* and upregulates SMAD7 levels. SMAD7 increased *ESRRB* promoter activity by upregulating MYC. Therefore, ESRRB, as a central link, forms a positive feedback loop with SMAD7 and MYC to promote cervical cancer development and progression. Thus, interrupting this loop may provide cervical cancer patients with novel therapeutic options in the future.

Authors' Disclosures

No disclosures were reported.

Authors' Contributions

Q. Li: Conceptualization, data curation, software, validation, investigation, methodology, writing–original draft. **P. Zheng:** Conceptualization, resources, supervision, funding acquisition, writing–review and editing.

Acknowledgments

The authors are grateful to Dr. Qingmei Liu (National Ministry of Education Key Laboratory of Contemporary Anthropology, School of Life Sciences, Fudan University, Shanghai, PR China) for providing pGL3-SBE4-Luc and pRL-SV40. This work was supported by a grant to P.-S. Zheng from the National Natural Science Foundation of China (nos. 81472728 and 81672910).

The publication costs of this article were defrayed in part by the payment of publication fees. Therefore, and solely to indicate this fact, this article is hereby marked "advertisement" in accordance with 18 USC section 1734.

Note

Supplementary data for this article are available at Cancer Research Online (http://cancerres.aacrjournals.org/).

Received January 18, 2023; revised May 10, 2023; accepted June 21, 2023; published first June 23, 2023.

References

1. Sung H, Ferlay J, Siegel RL, Laversanne M, Soerjomataram I, Jemal A, et al. Global cancer statistics 2020: GLOBOCAN estimates of incidence and mortality worldwide for 36 cancers in 185 countries. CA Cancer J Clin 2021;71:209–49.
2. Cohen PA, Jhingran A, Oaknin A, Denny L. Cervical cancer. Lancet North Am Ed 2019;393:169–82.
3. Smith EM, Ritchie JM, Levy BT, Zhang W, Wang D, Haugen TH, et al. Prevalence and persistence of human papillomavirus in postmenopausal age women. Cancer Detect Prev 2003;27:472–80.
4. Goodman A. HPV testing as a screen for cervical cancer. BMJ 2015;350:h2372.
5. van Dam PA, van Dam P-JHH, Rolfo C, Giallombardo M, Van Berckelaer C, Trinh XB, et al. In silico pathway analysis in cervical carcinoma reveals potential new targets for treatment. Oncotarget 2016;7:2780–95.
6. Martinez-Zapien D, Ruiz FX, Poirson J, Mitschler A, Ramirez J, Forster A, et al. Structure of the E6/E6AP/p53 complex required for HPV-mediated degradation of p53. Nature 2016;529:541–5.
7. Hoppe-Seyler K, Bossler F, Braun JA, Herrmann AL, Hoppe-Seyler F. The HPV E6/E7 oncogenes: key factors for viral carcinogenesis and therapeutic targets. Trends Microbiol 2018;26:158–68.
8. Zhou L, Qiu Q, Zhou Q, Li J, Yu M, Li K, et al. Long-read sequencing unveils high-resolution HPV integration and its oncogenic progression in cervical cancer. Nat Commun 2022;13:2563.
9. Cancer Genome Atlas Research N, Albert Einstein College of M, Analytical Biological S, Barretos Cancer H, Baylor College of M, Beckman Research Institute of City of H, et al. Integrated genomic and molecular characterization of cervical cancer. Nature 2017;543:378–84.
10. Lu Y, Li J, Cheng J, Lubahn DB. Messenger RNA profile analysis deciphers new Esrrb responsive genes in prostate cancer cells. BMC Mol Biol 2015;16:21.
11. Horard B, Vanacker JM. Estrogen receptor-related receptors: orphan receptors desperately seeking a ligand. J Mol Endocrinol 2003;31:349–57.
12. Adachi K, Kopp W, Wu G, Heising S, Greber B, Stehling M, et al. Esrrb unlocks silenced enhancers for reprogramming to naive pluripotency. Cell Stem Cell 2018;23:266–75.
13. Li X, Bu W, Meng L, Liu X, Wang S, Jiang L, et al. CXCL12/CXCR4 pathway orchestrates CSC-like properties by CAF recruited tumor associated macrophage in OSCC. Exp Cell Res 2019;378:131–8.
14. Clevers H. The cancer stem cell: premises, promises and challenges. Nat Med 2011;17:313–9.
15. Naik SK, Lam EW, Parija M, Prakash S, Jiramongkol Y, Adhya AK, et al. NEDDylation negatively regulates ERRbeta expression to promote breast cancer tumorigenesis and progression. Cell Death Dis 2020;11:703.
16. Yu S, Wong YC, Wang XH, Ling MT, Ng CF, Chen S, et al. Orphan nuclear receptor estrogen-related receptor-beta suppresses in vitro and in vivo growth of prostate cancer cells via p21(WAF1/CIP1) induction and as a potential therapeutic target in prostate cancer. Oncogene 2008;27:3313–28.
17. Gallagher KM, Roderick JE, Tan SH, Tan TK, Murphy L, Yu J, et al. ESRRB regulates glucocorticoid gene expression in mice and patients with acute lymphoblastic leukemia. Blood Adv 2020;4:3154–68.
18. Sun P, Sehouli J, Denkert C, Mustea A, Konsgen D, Koch I, et al. Expression of estrogen receptor-related receptors, a subfamily of orphan nuclear receptors, as new tumor biomarkers in ovarian cancer cells. J Mol Med (Berl) 2005;83:457–67.
19. Lei D, Yang WT, Zheng PS. HOXB4 inhibits the proliferation and tumorigenesis of cervical cancer cells by downregulating the activity of Wnt/beta-catenin signaling pathway. Cell Death Dis 2021;12:105.
20. Yang M, Yu H, Yu X, Liang S, Hu Y, Luo Y, et al. Chemical-induced chromatin remodeling reprograms mouse ESCs to totipotent-like stem cells. Cell Stem Cell 2022;29:400–18.
21. Padmanaban V, Krol I, Suhail Y, Szczerba BM, Aceto N, Bader JS, et al. E-cadherin is required for metastasis in multiple models of breast cancer. Nature 2019;573:439–44.
22. Wu T, Chu H, Tu W, Song M, Chen D, Yuan J, et al. Dissection of the mechanism of traditional Chinese medical prescription-Yiqihuoxue formula as an effective anti-fibrotic treatment for systemic sclerosis. BMC Complement Altern Med 2014;14:224.
23. Peng D, Fu M, Wang M, Wei Y, Wei X. Targeting TGF-beta signal transduction for fibrosis and cancer therapy. Mol Cancer 2022;21:104.
24. Colak S, Ten Dijke P. Targeting TGF-beta signaling in cancer. Trends Cancer 2017;3:56–71.
25. Yan X, Liu Z, Chen Y. Regulation of TGF-beta; signaling by Smad7. Acta Biochim Biophy Sin 2009;41:263–72.

26. Xie C, Wang F-Y, Sang Y, Chen B, Huang J-H, He F-J, et al. Mitochondrial micropeptide STMP1 enhances mitochondrial fission to promote tumor metastasis. Cancer Res 2022;82:2431–43.
27. Tewari KS, Sill MW, Long HJ 3rd, Penson RT, Huang H, Ramondetta LM, et al. Improved survival with bevacizumab in advanced cervical cancer. N Engl J Med 2014;370:734–43.
28. Ojesina AI, Lichtenstein L, Freeman SS, Pedamallu CS, Imaz-Rosshandler I, Pugh TJ, et al. Landscape of genomic alterations in cervical carcinomas. Nature 2014;506:371–5.
29. Madhu Krishna B, Chaudhary S, Mishra DR, Naik SK, Suklabaidya S, Adhya AK, et al. Estrogen receptor alpha dependent regulation of estrogen related receptor beta and its role in cell cycle in breast cancer. BMC Cancer 2018;18:607.
30. Fujimura T, Takahashi S, Urano T, Ijichi N, Ikeda K, Kumagai J, et al. Differential expression of estrogen-related receptors beta and gamma (ERRbeta and ERR-gamma) and their clinical significance in human prostate cancer. Cancer Sci 2010;101:646–51.
31. Garcia-Yague AJ, Rada P, Rojo AI, Lastres-Becker I, Cuadrado A. Nuclear import and export signals control the subcellular localization of Nurr1 protein in response to oxidative stress. J Biol Chem 2013;288:5506–17.
32. Ariazi EA, Clark GM, Mertz JE. Estrogen-related receptor alpha and estrogen-related receptor gamma associate with unfavorable and favorable biomarkers, respectively, in human breast cancer. Cancer Res 2002;62:6510–8.
33. Lu Y, Li J, Cheng J, Lubahn DB. Genes targeted by the Hedgehog-signaling pathway can be regulated by Estrogen related receptor beta. BMC Mol Biol 2015;16:19.
34. Tanida T, Matsuda KI, Yamada S, Hashimoto T, Kawata M. Estrogen-related receptor beta reduces the subnuclear mobility of estrogen receptor alpha and suppresses estrogen-dependent cellular function. J Biol Chem 2015;290:12332–45.
35. Pardali K, Kurisaki A, Moren A, ten Dijke P, Kardassis D, Moustakas A. Role of Smad proteins and transcription factor Sp1 in p21(Waf1/Cip1) regulation by transforming growth factor-beta. J Biol Chem 2000;275:29244–56.
36. Li Y, Li L, Qin J, Wu J, Dai X, Xu J. OSR1 phosphorylates the Smad2/3 linker region and induces TGF-beta1 autocrine to promote EMT and metastasis in breast cancer. Oncogene 2021;40:68–84.
37. Li J, Yuan J, Li Y, Wang J, Gong D, Xie Q, et al. d-Borneol enhances cisplatin sensitivity via p21/p27-mediated S-phase arrest and cell apoptosis in non-small cell lung cancer cells and a murine xenograft model. Cell Mol Biol Lett 2022;27:61.
38. Kowalik TF. Smad about E2F: TGF beta repressionof c-Myc via a Smad3/E2F/p107 complex. Mol Cell 2002;10:7–8.
39. Altomare D, Velidandla R, Pirisi L, Creek KE. Partial loss of Smad signaling during in vitro progression of HPV16-immortalized human keratinocytes. BMC Cancer 2013;13:424.
40. Strauss J, Gatti-Mays ME, Cho BC, Hill A, Salas S, McClay E, et al. Bintrafusp alfa, a bifunctional fusion protein targeting TGF-beta and PD-L1, in patients with human papillomavirus-associated malignancies. J Immunother Cancer 2020;8:e001395.
41. Zeglinski MR, Hnatowich M, Jassal DS, Dixon IM. SnoN as a novel negative regulator of TGF-beta/Smad signaling: a target for tailoring organ fibrosis. Am J Physiol Heart Circ Physiol 2015;308:H75–82.
42. Miyazawa K, Miyazono K. Regulation of TGF-beta family signaling by inhibitory smads. Cold Spring Harb Perspect Biol 2017;9:a022095.
43. Nakao A, Afrakhte M, Moren A, Nakayama T, Christian JL, Heuchel R, et al. Identification of Smad7, a TGF beta-inducible antagonist of TGF-beta signalling. Nature 1997;389:631–5.
44. Kleeff J, Ishiwata T, Maruyama H, Friess H, Truong P, Buchler MW, et al. The TGF-beta signaling inhibitor Smad7 enhances tumorigenicity in pancreatic cancer. Oncogene 1999;18:5363–72.
45. Kim YH, Lee HS, Lee HJ, Hur K, Kim WH, Bang YJ, et al. Prognostic significance of the expression of Smad4 and Smad7 in human gastric carcinomas. Ann Oncol 2004;15:574–80.
46. Millar SE. Smad7: licensed to kill beta-catenin. Dev Cell 2006;11:274–6.
47. Fan X, Wang Y, Jiang T, Liu T, Jin Y, Du K, et al. B-Myb accelerates colorectal cancer progression through reciprocal feed-forward transactivation of E2F2. Oncogene 2021;40:5613–25.